SHUTTLE TPS THERMAL PERFORMANCE AND ANALYSIS METHODOLOGY

W. E. Neuenschwander, D. U. McBride, and G. A. Armour
Space Transportation and Systems Group
Rockwell International
Downey, California

SUMMARY

Thermal performance of the TPS was approximately as predicted. The only extensive anomalies were filler bar scorching and over-predictions in the high Δp gap heating regions of the orbiter. A technique to predict filler bar scorching has been developed that can aid in defining a solution. Improvement in high Δp gap heating methodology is still under study.

Minor anomalies have also been examined for improvements in modeling techniques and prediction capabilities. These include improved definition of low Δp gap heating, an analytical model for IML convection heat transfer, better modeling of structure, and inclusion of sneak heating.

The limited number of problems related to penetration items that presented themselves during OFT have been resolved expeditiously, and designs have been changed and proved successful within the time frame of that program.

INTRODUCTION

The Space Shuttle orbiter thermal protection system (TPS) is designed to perform at least 100 missions before requiring major refurbishment. This is in contrast to the single-use designs for previous manned spacecraft heatshields such as Apollo. Basically, the protection against severe ascent and entry heating environments is composed of coated carbon panels, silica insulating tiles, and nylon felt blankets. The engineering task is further complicated where the system reaches interfaces with the various mechanical subsystems that are essential for launching, operating, landing, and servicing the vehicle. These interface areas are called TPS penetrations or singularities.

An overview evaluation of TPS thermal performance during the OFT program and of the analysis methodology is presented in this paper. Results of this evaluation will have value in the TPS thermal performance certification for more severe entry missions and TPS design of second-generation Shuttle-type spacecraft. TPS thermal performance assessments are based on postflight inspection results and measured TPS structure and component peak flight temperatures. These are compared with postflight developed analytical temperatures. Assessment of the analysis methodology is based on detailed comparisons of predicted temperature histories with measured data and evaluation of differences. Because their performance during the orbital flight test (OFT) program has not received as much publicity as that given the acreage tiles, the penetrations are granted some emphasis.

Included are the following: a summary description of the Columbia TPS design; thermal performance as evidenced by postflight inspections and development flight instrumentation (DFI) temperatures; and evaluation of thermal analysis methodology. Results are interpreted to reflect potential improvements in TPS thermal performance and analysis methodologies.

ABBREVIATIONS

AFRSI	advanced flexible reusable surface insulation
B/F	body flap
C/M	crew module
DFI	development flight instrumentation
ET	external tank
F/B	filler bar
FRSI	flexible reusable surface insulation
G/F	gap filler
HRSI	high temperature reusable surface insulation
IML	inner mode line
LRSI	low temperature reusable surface insulation
OFT	orbital flight test
OML	outer mold line
OMS	orbiter maneuvering system
OV	orbiter vehicle
PLB	payload bay
RCC	reinforced carbon-carbon
RCS	reaction control system
R/SB	rudder/speed brake
RSI	reusable surface insulation
RTV	room temperature vulcanized
SIP	strain isolation pad
STS	space transportation system

T/B	thermal barrier
TMM	thermal math model
TPS	thermal protection system

SYMBOLS

h	heat transfer film coefficient (Btu/ft^2·hr·^{o}F)
h'	heat transfer film coefficient at time of vent opening (Btu/ft^2·hr·^{o}F)
P	pressure
P'	compartment pressure at time of vent opening
p	local pressure (psf)
p_∞	freestream static pressure (psf)
$\dot{q}$	heat transfer rate (Btu/ft^2·sec)
$\dot{q}_s$	surface heating rate (Btu/ft^2·sec)
$\dot{q}(z)$	tile gap heating rate (Btu/ft^2·sec)
T_A	local air temperature (^{o}F)
T_A'	local air temperature at time of air vent opening (^{o}F)
T_o	initial temperature (^{o}F)
T_{SK}	structural skin temperature (^{o}F)
T_{STR}	structure
T'_{SK}	structural skin temperature at time of air vent opening (^{o}F)
T_t	peak surface temperature with turbulent boundary layer (^{o}R)
$\bar{t}_{s/s}$	equivalent thickness of structure skin and stringers (in.)
V	compartment flow velocity
V'	compartment flow velocity at vent opening
w_1	tile-to-tile gap width (in.)
z	dimension from heated surface (in.)
Δ	tile step dimension relative to adjacent tile (in.)
Δp	pressure difference across the tile
$\Delta\bar{t}$	delta heatsink capability of $\bar{t}_{s/s}$ due to nearby heavier structure (in.)
δ	tile thickness (in.)
ψ	filler bar scorching parameter

TPS GENERAL DESCRIPTION

The OFT vehicle Columbia, Orbiter 102, employs four basic thermal protection materials: reinforced carbon-carbon (RCC), high temperature reusable surface insulation (HRSI) tiles, low temperature reusable surface insulation (LRSI) tiles, and flexible reusable surface insulation (FRSI) blankets. These have been discussed in detail in references 1 through 5. Figure 1 shows the location of the acreage TPS materials on the orbiter and figure 2 shows typical penetrations. The list of the penetrations given in table I shows that the TPS is more complex than just tiles and FRSI blankets even though the penetrations comprise only a fraction of TPS surface area.

The basic TPS was designed to protect the primary structure from exceeding 350°F (the 100-mission temperature limit). The design was developed employing a minimum-weight engineering approach; that is, there was no intentional conservatism in the entry trajectory, heating or thermal analysis methodologies. However, the design was based on a single-orbit type mission that yields higher structure temperatures at the start of entry. This would be the case for a once-around abort, but the TPS was not designed to an abort as is sometimes believed.

Establishment of and design to material temperature limits were of prime importance. These criteria include those for the basic TPS materials illustrated in figure 3, and also cover about 50 other materials predominately used in the penetrations. Typical limits are shown in table II. There are a number of exceptions as illustrated by the following examples. AB312 ceramic fabric, used for gap filler/thermal barrier covers, has a nominal 2000°F limit, but its use is acceptable to 2300°F and 2600°F for ten and one missions, respectively. High-density HRSI (LI-2200) has been certified to 2900°F by arc-jet testing for at least one mission at a worst-case environment predicted in the gap between the elevons and the fuselage. On the other hand, titanium mounting flanges on the reaction control system (RCS) thrusters are limited to as low as 400°F to protect adjacent components.

The TPS and structure were instrumented with thermocouples and other temperature-sensing devices to provide data for thermal performance verification of the TPS for operational missions more severe than OFT missions. Figure 4 shows representative installations of the flight instrumentation plus number and locations of temperature measurements.

Unique designs in the TPS are called penetrations or singularities. These include the hatches and actuated doors, windows, aerodynamic control surfaces, RCS and orbital maneuvering system (OMS) thrusters, main engines, overboard vents and drains, umbilical connections, service access panels, and structural lifting and attach points (see table I). Around them the TPS is comprised of components made from numerous temperature-resistant metals, ceramics, plastics, and elastomers, which have been formed, cast, extruded, woven, and laminated. Penetrations to be discussed are located on the orbiter, as indicated in figure 2. They include the external tank (ET) umbilical door, a payload bay door bare hinge, selected rudder/speed brake components, the aft fuselage stub and body flap, one location in the wing/elevon seal system, primary thrusters in the forward RCS, and the windshield.

FLIGHT TEST RESULTS

OFT Entry Conditions

Example comparisons of surface temperature responses are shown in figure 5 for a lower surface mid fuselage location. These comparisons depict trajectory effects at the time of boundary layer transition to turbulent flow as evidenced by the rapid increase in surface temperature in the 1000- to 1300-second time frame. As shown, the turbulent spike temperatures occur earlier for each successive OFT flight, and the turbulent spike heating rate is indicated to increase as transition time decreases. This general trend is typical for the orbiter lower surfaces.

Acreage TPS

For the most part, the OFT heating environments were rather mild relative to the capability of the TPS. This is illustrated by the STS-2 peak surface temperatures shown by figure 6. STS-4 experienced higher peak turbulent temperatures, as illustrated by figure 5; however, these are not shown because of limited data (not available until about 1000 seconds after the entry interface.) Peak temperatures of the filler bars (F/B), strain isolation pad (SIP), and structure from STS-2 DFI are presented in figure 7. All peak temperatures are noted to be considerably lower than the 100-mission design allowables. These temperatures are typical of those for all flights. A comparison of peak structure temperatures for all flights is presented in figure 8. These temperatures are about the same, ± 25°F for all flights, and well below the 350°F, 100-mission allowable.

TPS Penetrations

It is not feasible to discuss flight data from all the instrumented penetrations, so three were chosen for this section as being illustrative. They are an ET door, a payload bay door hinge, and the rudder/speed brake conic seal and structure.

The ET is connected to the orbiter through two umbilical panels located on either side of the lower centerline just behind the aft fuselage bulkhead. Structural attachments, various propellant lines, and a number of electrical connections pass through these panels. During ascent, the ET umbilical doors are held open by latches located at the centerline. After the ET is jettisoned, the doors are closed to protect the umbilical panels. Each door is attached to the fuselage with two bare hinges, which are flush with the outer mold line (OML). The outer surface of the door when closed is covered with HRSI. A thermal barrier, which runs around the periphery of each umbilical well, protects the structure from entry aerodynamic heating and accommodates relative movement between the door and fuselage. Pressure seals between the doors and structure and flow restricters along the door edge tiles complete the local TPS. The ET door/fuselage interface is depicted in figure 9. The doors are made from beryllium for stiffness, reduced weight, and to obviate the need for insulation blankets, which would be exposed to destruction during ascent. Even though the beryllium could tolerate almost twice the temperature, the thermally critical component for the doors is the 550°F HRSI/SIP bondline limit. At this location the thermal barrier consists of an AB312 cover and sleeve with an internal Inconel (International Nickel Company) X-750 knitted wire spring.

Flight temperatures for three DFI are shown in figure 10. It can be seen that the thermal barrier cover temperature neared its long term limit on STS-1 and may have been dropping from a peak above 1600°F on STS-4 when post-blackout data were acquired. The HRSI tile DFI recorded temperatures well below the limit, but this would be expected because it is located in a tile sidewall below the OML. The door remained relatively cool.

The payload bay doors are attached to the fuselage by 13 external hinges on each side. The six forwardmost hinges, which experience the most severe heating, are covered to protect them. The covers are made of Inconel and are designed to permit the doors to open without any restriction on movement. Since the predicted baseline aerodynamic entry heating was sufficiently lower, the remaining external hinges were left unprotected to reduce complexity. The gaps between the doors and fuselage are filled with a silica fiber brush thermal barrier. This protects the door structure and the environmental seal from direct convective heating and also accommodates structural movement (see figure 11).

STS-1 through STS-4 DFI temperatures for the most forward unprotected hinge are presented in figure 12. One DFI is on the forward clevis facing the oncoming flow. Recorded maximums were well over the 1200°F criterion for this instrument on two missions; however, readings were erratic, and poor contact between the sensor and clevis was suspected. Postflight inspection of the sensor indicated that it was attached but the amount of contact area with the clevis could not be determined. Because it was uncertain if the DFI data actually were a true indication of the clevis temperature, authority was issued to remove pins on hinge 7 (maximum temperature) and hinge 9 (lowest stress margin), inspect the dry lubricant (limit 1000°F), and run hardness tests on pin 7. The results indicated no degradation caused by excessive temperature exposure and no loss of strength. In order to eliminate direct stagnation-type heating on the DFI, a piece of filler bar was placed over the sensor for STS-2 and STS-3 and replaced prior to STS-5. The below-limit readings on these flights are more accurate measurements of the clevis temperature. Temperatures at the clevis/fuselage interface remained low and changed little from flight to flight. The hinge lug is exposed to far less aerodynamic heating, and its DFI is located in a cavity between tiles. These facts are reflected in the much lower lug temperatures (compared to the clevis) plotted in figure 12.

As illustrated in figure 13, the vertical tail consists of a fixed structure, the fin, and two moveable surfaces that have the capability of acting together as a rudder or separately as a speed brake. At the hinge line a gap exists to permit movement of the rudder/speed brake with respect to the fin. In addition to external LRSI and HRSI, the structure must be thermally protected by closing the gaps along the hinge line and around the rudder/speed brake perimeter with a system of seals. The most visible element is the Inconel conic seal, which acts as a rub surface for seals attached to the fin trailing edge and the rudder/speed brake leading edge. Other seals are found at the top and bottom of the cone as well as between rotating sectors. Around the perimeter, there are seal requirements in the gaps between the fin and the rudder, along the rudder/speed brake trailing edge, and at the split line between upper and lower panels. The aforementioned seals are made from several combinations of flat metallic springs, insulation-filled ceramic sleeving, graphite blocks, and knitted wire springs.

There are several DFI on the conic seal. Readings from two of them are plotted in figure 14. Both sensors are located on the inner face sheets of the Inconel honeycomb. One is forward near the fin seal, and the other is aft but at the predicted point of maximum interference heating when the rudder/speed brake is closed during entry. Conic seal temperatures stayed well below the 1250°F limit. The gentle rise in the aft sensor DFI data to only about 250°F indicates that it is behind the rudder/speed brake leading edge seal rather than forward of it in the more severely heated position described above. More rapid increases, although to lower levels, are seen for the structure instrument located near the rudder/speed brake trailing edge. This behavior is as expected for metallic surfaces that are directly exposed to a small amount of wake heating when the rudder/speed brake is opened at Mach 10.

TPS Thermal Anomalies

Postflight inspections have shown every flight to have had some local anomalies. Table III identifies the general types of heat protection anomalies that have been observed during inspections. Figure 15 identifies the locations of those that are most significant. Most anomalous conditions are easily detectable by visual inspection of the OML; however, some require removal of access panels and/or more detailed inspections.

Priority attention has been (and is) given to understanding and preventing anomalous conditions that require detailed inspection. Some design changes have already been implemented to alleviate these problems. Certain tile gaps near the wing trailing edge have been filled to reduce air flow into the elevon cove, and the internal insulation has been changed from FRSI to AFRSI. Designs of the edge tiles of the gear and ET doors have been modified to restrict subsurface flow. In some cases, repairs have been made to the existing design. An example of this is in the body flap stub plate tiles.

One anomaly of concern that requires detailed inspection is filler bar (F/B) scorching between lower surface tiles. At several hundred randomly distributed locations, filler bars reached 950°F to greater than 1375°F where 400°F to 500°F were predicted. Filler bar scorching has occurred on every flight. A summary of occurrences and scorch severity is presented by Table IV. Some filler bar scorching is known to be caused by structure leakage, e.g., around doors. These can be eliminated by design change or local repairs. Scorching in the general acreage is a probability event depending on certain combinations of tile steps and gaps, heating/boundary layer conditions, and tile-to-filler bar gaps. Eliminating filler bar scorching in the acreage regions is a more complex problem.

Since multiple reflights of scorched filler bars could result in structural damage, degraded ones are repaired after each flight. They are mostly repaired by filling the gap with room temperature vulcanized (RTV) impregnated ceramic fabrics (Ames gap filler). When severely degraded, the filler bars are replaced, and this requires tile removal. The repair effort is relatively simple, but the problem is that many thousands of gaps have to be inspected just to find a few hundred scorches that require repair. This inspection has been required because, until recently, the cause wasn't quantitatively defined and step/gap allowables (criteria) that would preclude filler bar scorching could not be developed.

Continued examination of flight data resulted in identification of a correlation parameter that distinguishes between step/gap combinations that cause scorching and those that do not. The parameter is

$$\psi = (T_t/1000)^{0.5} \left(\Delta^{.5} + w_1^{.83}\right)/\Delta^{.12}\delta^{.5}$$

This parameter correlated a statistically representative sample of scorched filler bar data to within ±20 percent. The lowest value was 0.41 and corresponds to a filler bar temperature of about 950°F which is the threshold of visual detection of a scorch per inspection criteria and NASA JSC plasma-arc test results. The ψ value for 800°F, the 100-mission limit, was identified to be 0.38 from a combination of flight and plasma-arc data. With these analysis results, tile step/gap criteria can be defined that will preclude filler bar scorching.

Unfortunately, implementation of an absolute no-scorch step/gap criteria has only theoretical feasibility. Analysis of data indicates that about 20 percent of scorches were caused (or highly influenced) by aft-facing steps on adjacent tiles. Step/gap criteria involving multiple tiles would be difficult to apply and execute with confidence. Other practicality problems exist. These include the fact that future worst-case trajectory/heating environments are required to define criteria, but are not presently known, and inspection/repair for scorched filler bar is not included in the planned orbiter turnaround schedules. At the time of this writing, the best program solution to this problem is under study.

The body flap is attached to the aft fuselage stub and driven in its trim control function by rotary actuators. In addition to HRSI tiles that cover the exterior of the stub and body flap, there are a number of seals that prevent direct flow and resultant convective heating from passing from the high pressure lower surface to the low pressure wake region. There is the hinge seal, consisting of Inconel 718 panels, which covers the entire width from stub to stub, closing off the lower cove. So-called chain seals block flow around the ends of the stub. The design for thermal barriers between the body flap and tiles and the stub consists of knitted wire springs within AB312 covers. All of the above are or have ceramic cloth components that bear on aluminum heat sinks attached to each end of the fuselage stub. These are known as the rub plates (see figure 16).

A temperature sensor on the left-hand body flap rub plate exhibited a rapid rise to 395°F after communications blackout during STS-1 entry (see figure 17). This behavior was unexpected because the rub plate is heavy. The peak also constituted an overtemperature since the 100-mission aluminum material limit is 350°F. No other overtemperatures were recorded in the area, although the output of another DFI on the upper end of the plate also rose and fell rapidly. Postflight visual inspection of the exterior revealed no particular evidence of overheating. Observed aluminum temperatures were used as drivers in the thermal math model (TMM) along with postflight predicted heating. Stress analysis personnel used output from this work and came to the conclusion that no structural degradation had occurred during STS-1. A later visual inspection revealed gaps between the tiles at the lower, outboard corner of the stub. It was surmised that sneak flow entered at these points, directly heated portions of the rub plate bounded by the hinge and chain seals, and exited at a lower pressure area—perhaps the upper cove. For STS-2, the aforementioned gaps, which were tapered in-depth, were plugged with Ames fillers to preclude the flow.

Again on STS-2, the rub plate DFI rose rapidly and went over temperature to 405°F. Because the shapes of the temperature-versus-time curves were almost identical for both flights, it was evident that the Ames gap fillers installed after STS-1 did not cure the anomaly. Carrier panel tiles were removed from the left-hand stub. As shown in figure 18, a section of charred and missing filler bar was found. The corner of the rub plate adjacent to this section was discolored indicating excessive temperatures. There was also evidence of a forward-facing CML step between these tiles. Prior to STS-3, the missing filler bar was replaced, and nearby pad gap fillers were rebonded. The stepped tile was not refurbished.

Figure 17 reveals that the left-hand rub plate temperature followed a repeat history during STS-3. As noted, a new flow barrier was added along with the pad gap filler, and two lower surface tiles were remade to remove the forward-facing step. Finally, on STS-4, the maximum temperature was what had been expected for a heavy aluminum plate; however, the STS-5 temperature history, while not exceeding the 350°F criteria, looks familiar. More extensive tile changes have been designed to permit use of full-depth pad in place of Ames gap filler, and these are being installed during the modification period.

The elevons provide orbiter flight control in pitch and roll during atmospheric entry flight. They are divided into two segments for each wing, and each segment is supported by three hinges (two fixed and one actuator). The seal system design must permit the required control surface motion and yet prevent the destructive flow of hot plasma from the lower to upper surfaces through the wing/elevon interface. Basic features are shown in figure 19, a section normal to the hinge line. The lower surface is protected by sculptured HRSI with a nominal 0.5-inch gap between wing trailing edge and elevon leading edge tiles. The lower, internal cavity is closed out by primary and redundant seals. Spring-loaded polyimide blocks bearing on aluminum and Inconel rub tubes make up the primary seal while reinforced silicone elastomer sheets form the redundant seal. Together, the aforementioned penetration is known as the elevon lower cove. Also depicted in figure 19 is the closeout to the upper wing-to-elevon cavity, commonly known as flipper doors and rub panels. This TPS is insulated hot structure made from titanium and Inconel on the inboard and outboard elevons, respectively. The wing/elevon seal system takes on its greatest complexity when a chordwise interruption occurs at the inboard and outboard ends of each elevon and at each hinge and actuator.

There have been some temperature-related problems with the elevon lower cove, but none that brought forth safety-of-flight concerns. STS-1 postflight visual inspection of the closeout panel FRSI insulation revealed evidence of spanwise and/or leakage flow within the coves. There were areas of scorching and charring, particularly at the outboard elevons. This is illustrated in figure 20, which is a view looking up with the wing trailing edge and elevon leading edge tiles removed. Physical evidence revealed that flow entered the gap between wing and elevon tiles and exited near the stubs and actuators. After the first flight, the insulation on the closeout panels was changed from FRSI to higher temperature capability AFRSI. In addition, Ames gap fillers were placed between the tiles immediately upstream of the trailing edge tiles and thicker SIP was added to improve seating of these tiles.

Some anomalous behavior of elevon lower cove DFI was noted, but they recorded no overtemperatures. Time-temperature histories of the sensor on the primary seal tube at 90 percent half span are plotted in figure 21. The shapes have more pronounced peaks than would be expected in pure soakback situations. This is ascribed to the direct, low level convective heating that caused the FRSI degradation. The heating is thought to have come about from the spanwise flow mentioned above and from sneak circuit flow under the wing trailing edge tiles. Also note in figure 21 that seal leakage measurements in this region have generally declined. All in all, it would appear that the elevon lower cove seal system on Columbia is currently functioning as designed.

Including the payload bay door bare hinge overtemperatures, which were described earlier as instrumentation installation problems, three anomalous penetrations situations have been discussed. This points out that, considering the hundreds of penetrations and singularities, there were a minimal number of temperature-related discrepancies during the OFT program.

EVALUATION OF THERMAL ANALYSIS METHODOLOGIES

Assessment of analysis methodologies is being performed by comparing analytical results with flight measurements. Discrepancies between flight and calculated temperatures using design methodologies are examined for cause. When a discrepancy appears to result from analytical modeling, the technique is examined for potential improvement. In the case of acreage TPS, the orbiter is surveyed to assess data consistency of discrepancies and modeling improvements. However, for penetrations the analysis is mostly unique to a specific penetration.

Acreage TPS

Nodal TMM's are used for flight temperature predictions. A design model for a 1.0-inch tile would have about 120 LI-900 nodes or about 240 LI-900 nodes for a 3.0-inch tile. Nominal thermophysical property data are used for all TPS and structure materials.

Nodal models of tiles are three-dimensional and include simulation of the SIP and filler bars. Gap heating is applied to the tile sidewalls. For low pressure gradient regions of the orbiter, the gap heating varies with surface heating rate and dimension from the tile surface. For high pressure gradient regions with open gaps (i.e., wing glove, aft chine, forward fuselage, and elevons), the gap heating is also a function of pressure and pressure gradient in direction of the open gap. High pressure gradients are defined as $p^{1/2}\ dp/ds > 1.06\ psf^{3/2}/inch$.

The structure is modeled to include the effective thickness of skin, and stringers ($\bar{t}_{s/s}$) and the thermal capacity of nearby heavier structure (i.e., frames). Honeycomb structure is modeled as honeycomb. The structure inner mold line (IML) is assumed to be adiabatic.

The FRSI design nodal models are one-dimensional with nominal thermal property inputs. Structures are modeled as described.

Postflight analyses have been performed using these design methodologies to assess the TPS thermal performance and the adequacy of the analytical models for flight certification. Although there have been some anomalies, the overall TPS thermal performance and analysis adequacy appears acceptable. Peak temperatures of SIP and structure, as measured by the DFI, are well within design allowables. This is illustrated by figure 22, which also shows that calculated temperatures, using actual flight surface heating, are in reasonable agreement with measured data. These temperatures, shown for STS-2, are typical of those for all OFT flights.

Detailed examination of the DFI and analysis data shows some discrepancies not indicated by peak temperatures. Temperature history comparisons are shown by figures 23 through 27. These are rather typical results. Figure 23 illustrates that the high pressure gradient gap heating is quite conservative. Calculated tile sidewall, filler bar, and structure temperatures are all well above the measured. Gap DFI in high Δp regions is very limited. However, at several high Δp locations, surface and structure skin measurements are available. Analysis at these locations shows similar conservative disagreement with structure temperatures.

In low pressure gradient regions, the trend is for the temperature rise rates of SIP and structure to be greater than calculated. But the agreement is reasonably close and the analytical conservatism of the cool down compensates for the rise-rate optimism. Figures 24 and 25 illustrate this observation.

Figure 25 implies another analysis anomaly that also shows up at other orbiter locations: the calculated in-depth reusable surface insulation (RSI) temperatures are conservative but the SIP and structure temperatures are optimistic. This could be interpreted to mean that the low gap heating in the analysis is optimistic; however, figure 25 shows this gap heating to be reasonable until late in the entry (to about 1200 seconds). The LI-900 temperature measurements are suspect. It is speculated that launch vibroacoustics resulted in the thermocouples cavitating the LI-900 such that they were not in contact with LI-900 at the thermocouple junction. That this could happen was evidenced in a vibroacoustic test performed at NASA Langley where thermocouple wires were observed to have cavitated LI-900. Other explanations (e.g., LI-900 conductivity variation with temperature, hot air ingestion at the base of the tile) were considered improbable following analysis.

Examples of thermal response at upper surface locations are presented by figures 26 and 27. Figure 26 shows the thermal response at an LRSI location. The calculated SIP and structure rise rates are slightly lagging measured temperatures. (Note also the contradiction by the LI-900 temperatures.) Figure 27 shows the thermal response at an FRSI location, where again calculated temperatures are lagging measured temperatures. Both the examples show good agreement with peak temperatures and cool down rates. This is typical of upper surface locations with the thinner TPS.

In summary, the acreage TPS design methodologies produce peak temperatures that are conservative and adequate for Eastern Test Range flight certifications. However, this conservatism results from compensating effects of optimistic and conservative thermal modeling techniques.

Modeling improvements are being evaluated to show better agreement with flight data and include structure modeling, low pressure gradient gap heating, and IML convection. Also, the tile models have a finer nodal network of the SIP and filler bar.

The design method of structure modeling was to use an effective structure thickness that included both the skin stringer and $\Delta\bar{t}$. The new method connects $\Delta\bar{t}$ to $\bar{t}_{s/s}$ with a contact resistance to increase the rise rate of the structure skin. Values were empirically established. The value for the lower fuselage is 1.0 Btu/ft^2·hr·°F. For other locations except lower wing, the coefficient is 0.2 Btu/ft^2·hr·°F. At time of this writing, the lower wing modeling is still under study.

A pressure dependent, low pressure gradient gap heating model was developed that improves agreement between flight and analysis data. The model is

$$\dot{q}(z)/q_S = (1.0 + p/20)^{1.4\sqrt{z}} \times (\dot{q}/\dot{q}_S)_{des.\ extended}$$

The $1.4\sqrt{Z}$ exponent is truncated at a value of 1.85. The design gap heating and design extended distributions are presented by figure 28. The pressure factor gets to be a large number for higher pressures and thick tiles. Even so, at later entry times when the gap heating is negative, the pressure factor is not large enough to match gap cool down rates.

The orbiter interior is repressurized by air vent air, which has a marked effect on structure temperatures. Air vents open at 2400 fps orbiter ground speed, which is typically about 85,000 feet altitude. From flight and analysis results, hot structure (skin) is cooled and cold structure is heated by the ingested air.

A heat transfer convection model was developed from examination of flight and venting analysis data. The modeling analysis was difficult to accomplish because of lack of direct data. The heating/cooling is a function of three parameters that are dependent on each other and vary with time:

$$\dot{q} = h\ (T_{STR} - T_A)$$

Nonetheless, based on a DFI air temperature measurement and a high density of structure thermocouples at BP1801, a heat transfer model was developed.

$$h = h'\left(\frac{P}{P'}\ \frac{T'_A}{T_A}\ \frac{V}{V'}\right)^{1.6}$$

Air temperature (T_A) is defined to vary linearly with time between compartment air at the time of air vent opening and ambient air temperature at touchdown at the landing site. Air temperature at air vent opening time is approximated as

$$T'_A = T_o + 0.1\ T'_{SK}$$

The film coefficient at air vent opening, h', was empirically defined to be 0.07 Btu/ft^2·hr·°F for LI-insulated structures and 0.10 for uninsulated structures.

Compartment pressure is a function of freestream static pressure, as shown by figure 29. Velocity ratio (V/V') is defined in the same figure for STS-2. Extrapolation of the STS-2 velocity parameter to other trajectories uses the following relationship:

$$V/V' = [\dot{p}_\infty/(\dot{p}_\infty)_{STS-2}]\ (V/V')_{STS-2}$$

This extrapolation technique was used to calculate STS-3 structure temperatures. It showed that the agreement was reasonably good (about the same as the STS-2 data agreements).

Overall, the modeling improvements yield better structure temperature rise rates and peaks. Also, the shaping of the SIP temperature response and peaks are also better; however, in some cases there is very little improvement over results from the design models. This is usually the case for the thinner TPS and locations where $\Delta\bar{t}$ is small compared to the structure skin-stringer thickness.

Assessment of these modeling improvements has been made by comparing analytical and measured temperatures at 47 locations for STS-2 and 25 locations for STS-3. The agreement is quite good for the fuselage, OMS pod, and vertical tail low pressure gradient regions. Modeling of the wing TPS and structure is still under study.

The agreement between analytical and measured temperatures is illustrated by figures 30, 31, and 32 for the fuselage lower surface. Figure 30 is for a forward fuselage location where the IML is insulated. Peak temperatures are in good agreement and the response shapes for the filler bar, SIP, and structure skin are quite acceptable. The deviation between the filler bar temperatures after the peaks is caused by the convective gap cooling being greater than calculated even though the pressure factor in the gap heating model is large. Figures 31 and 32 compare temperatures at an uninsulated location. Again, structure skin and SIP temperatures are in agreement. The calculated filler bar temperature appears to be conservative; however, it is not known if the filler bar thermocouple is located in an open gap.

Temperature comparisons at upper surface locations are shown by figures 33 and 34. The calculated structure temperature on the vertical tail lags the measured temperature by about 10°F, but the peak is good. The OMS pod structure temperature also lags the measured temperature by about 50°F, but the peak is in good agreement. On the OMS pod the calculated cool down rate is greater than measured.

In most cases, the modeling improvements yield better agreement with flight temperatures than the methodology used for design. This is particularly evident in comparison of structure temperatures in regions of high heat load where the tiles are thick. In these regions, such as the lower wing, IML cooling helps to offset a rather significant increase in structure temperature from heat soakback from the tiles.

More modeling improvement analysis is in process. The structural backface of the three-dimensional tile model could use improvement to better account for radiative interchange between the upper and lower wing structure. Even with the modeling improvements described, the lower skin temperature rise rates are optimistic and the cool down conservative. Another area of modeling improvement is with the high pressure gradient gap heating since the design method appears to be very conservative.

Penetrations

The general approach to a penetration thermal analysis required identification of the physical location and configuration, applicable heating and other boundary conditions, and subsystem operating parameters. To physically represent the penetration, the structural and TPS cross-section of the installation was subdivided into a sufficiently fine matrix to represent it as a TMM in the computer thermal analyzer program. Baseline models represented nominal design configurations. Limit case heating and other boundary conditions were also identified and formatted for computer input. These included various combinations of the following:

1. Initial temperatures either prelaunch or pre-entry after specified orbital operation

2. Predicted ascent and entry aerodynamic heating at all OML areas and within the penetration

3. Ascent radiative heating from the booster and main engine plumes, and recirculation convection effects from the latter source

4. Local RCS and OMS engine plume heating during system operation

5. External reradiation or radiation interchange within the penetration and/or internal to the orbiter

6. Miscellaneous system operating parameters (e.g., ablation, internal heat generation, fluid flow, and cabin conditioning)

The complexities of the installations typically dictated the use of two-dimensional TMM's based on the worst case location in each individual penetration rather than more comprehensive models; however, limited three-dimensional models were forced in a few situations, while other cases were simple enough to represent in one dimension.

The basic TPS sizing was accomplished based on minimum insulation thickness requirements for each given orbiter location without regard for special situations such as penetrations and singularities. Further design constraints required the penetrations to be thermally controlled passively and independent of internal systems for cooling. All in all, these ingredients imposed challenging design conditions on these TPS features.

Postflight evaluations consisted of screenings that categorized results as to their criticality. First priority was given to components that exceeded their design temperature limit. Two examples were discussed in previous sections: the payload bay bare hinge and the fuselage stub rub plate and body flap. Second came those that exhibited anomalous readings that were considered problems even though they stayed below criteria. Instances include the wing/elevon lower cove, which was mentioned earlier and will be discussed further in the following, and the RCS installation, which is covered in this section. Because of the limited time and resources, the least attention could be devoted during the flight test program itself to DFI readings that were overpredicted.

The canopy windshields have obvious functional requirements, serving as the pilots view ports during launch, landing, and other operations. There are a total of six windshields with each window assembly consisting of three high temperature glass panes. Figure 35 depicts a sample cross-section. The outer pane of each set is fused silica glass, which serves as a heat shield and is sealed to prevent hot gas plasma from penetrating into the internal structures. The middle window pane is also fused silica and serves as a fail-safe redundant member to either the outer thermal pane or the inner pressure pane. The inner pane is heat-tempered aluminosilicate glass and is the primary pressure containing pane for the cabin atmosphere. All glass surfaces are coated except for those of the thermal (outer) panes. Special HRSI (LI-900) tiles that overhang the outer window frames protect the aluminum canopy structure. The HRSI is bonded to 0.09-inch SIP, which is, in turn, bonded to carrier panels. These assemblies are mechanically attached to the frames. Captive-type gap fillers are installed between the tiles. AB-312 cloth filler, bonded only to the carrier panels, supports the overhanging portions of HRSI. To prevent the inflow of hot plasma during entry and the possible leakage of cabin pressure, thermal barriers and pressure seals were incorporated into the window design. The external thermal barriers are made of woven ceramic fiber. For external pressure seals, fluorocarbon O-rings are used. The crew module windows (redundant and pressure panes) are contained in frames having steel, aluminum, and beryllium components. The crew module window frame is actively cooled by water flowing in pairs of tubes around each window's inboard perimeter. Environmental barriers having rigid and flexible portions are located between the canopy and the crew module. At highly heated windshield locations, insulated heat shields are required to protect the flexible purge barrier. In turn, the crew module wall requires TCS insulation blankets to protect it from radiating surfaces.

Figure 36 shows DFI data and analysis time-temperature histories for a location at the downstream region of the middle windshield. On STS-2, the preflight work substantially overpredicted the bondline DFI early in entry. A comparison between prediction and data at the OML surface indicates a probable cause for the bondline error: the experienced aeroheating did not have an early high load period but did display an unexpected peak. Heating rates were derived from surface DFI data and extrapolated to the window pane surface and the overhanging tile sidewall. These were then used in the baseline TMM. As shown by the solid line in the figure 36 plot, a much improved correlation at the bondline was achieved.

The situation regarding STS-3 was similar. Just as the preflight prediction of aeroheating was better, so was the thermal analysis output. Again, an improved overall match between predicted bondline temperature and data came from using derived heating. Even though the bondline value is slightly undercalculated (<25°F) at its peak and falls less rapidly than the data, the basic validity of the TMM has been demonstrated.

The forward RCS provides attitude control and small velocity increment translation from main engine cutoff during ascent until the entry interface. It includes 16 radiation-cooled thrusters (14 primary and 2 vernier), made predominantly from columbium (disilicide coated except for the injector plates), and fully exposed to aerodynamic heating. Surrounding HRSI tiles of the TPS have been partially replaced by other materials. Insulation-filled metallic plume shields are placed downstream of long scarf (primary -Z and -X and vernier) thrusters. High

density (22 pcf) RSI tiles form the TPS in narrow areas between the -Z, ±Y, and -X thrusters. Thermal barriers serve to block gaps between nozzle exits and adjacent TPS from hot boundary layer gases. Other thermal barriers are required between the plume shields and surrounding tiles. Each thruster is housed within a cylindrical titanium container that seals the internal compartment from the exterior environment. The design is complex. There are approximately 20 maximum temperature limits to be observed, many with several variations associated with position, mission phase, or frequency of occurrence. The primary downfiring (-Z) thrusters experience the most severe entry heating. A section through the downstream edge of this installation is shown in figure 37.

A DFI is located on the inside of the plume shield adjacent to the thermal barrier. The recorded sudden rise in entry temperatures on STS-2 was not predicted by the baseline TMM employing postflight nominal aeroheating. This can be seen by comparing the solid curve with the data symbols (filled circles) in figure 38. The response is little different than the STS-1 experience reported in reference 1.

Several revisions were made to the TMM after studying thermal flight data from the region and the postflight inspection reports. First, the as-built configuration (thermal barrier recessed inside the OML and rounded) and expansion characteristics of the plume shield were considered. This exposed additional areas of the sealing surface to direct aeroheating and altered the perturbation and gap heating factors. Second, interpolation between the data from the closest surface DFI was used to estimate actual reference heating. Third, the plume shield DFI itself was added to the TMM at its design location. With the revisions, a much better prediction of STS-4 data was obtained, as indicated by comparing the dashed curve to triangle symbols in figure 38. Peak values are well matched as is the time-temperature history following the peak. The early overprediction is thought to be caused by the shape of the derived aeroheating curve. The forward RCS thruster TPS TMM is considered sound.

Flight data from a DFI in the wing/elevon lower cove was presented earlier (figure 21) along with a description of this penetration area. A series of TMM updates have markedly improved the ability to predict temperatures for future entry environments. Figure 39 shows that the baseline was poor at anticipating both the peak and shape of the recorded data. One of the first changes included correcting the sensor location. Since it was obvious from postflight inspections that direct convective heating was present in the cove, several low percentage values of OML reference heating were applied to appropriate TMM internal sections. This produced predictions that bracketed the data. Although the assumed levels of sneak flow heating were slightly higher than that correlated from ground tests, they seemed quite believable in light of the FRSI degradation in the first OFT flight. Finally, an intermediate level of sneak heating was combined with cooling correlations developed for air flow following the vent opening. As demonstrated by the solid curve in figure 39, the validity of the current TMM is much better.

CONCLUSIONS

Overall, flight data show the TPS design and thermal performance to be quite good and the thermal analysis methodologies adequate. Examination of physical and analytical data has identified some elements of the design and methodologies that could have been better if data had been available on which to base improvements.

LESSONS LEARNED

Results revealed that some technology inadequacies exist. Their identification could benefit future design and analysis of spacecraft heat protection systems.

Low Δp gap heating is a function of pressure level. This wasn't known before STS-2. Ground test facilities did not have the capability to produce data to identify effects of pressure level and theory (engineering methodology) did not identify pressure level as a significant parameter. This knowledge could have affected TPS design. Filler bar scorching is caused by abnormally high rates of gap heating. These high heating rates are pressure-level dependent and the significance of pressure level is amplified with boundary layer disturbances caused by tile steps. If this had been known before the first flight, filler bar scorching would have been expected and step/gap criteria for prevention identified; however, it is most probable that these criteria would have not prevented about 20 percent of the filler bar scorches, and would not have eliminated detailed postflight inspection for the scorched filler bars. As such, it is likely that this ignorance was to the advantage of the STS program in its preflight stage. Now, however, gap heating sensitivities to pressure level and tile step/gap dimensions are all recognized and should be considered in future ground testing of similar TPS configurations. This suggests that consideration should be given to upgrading the flight simulation capability of plasma-arc test facilities.

Other inadequacies relate to the IML convection heat transfer phenomena. Per interpretation of flight data, the governing heat transfer relationships deviate considerably from theoretical expectations. The air temperature and heat transfer coefficients are predominantly influenced by the local structure temperatures (hot and cold) with little remembrance of prior temperature/boundary layer history. Also, the variation of heat transfer film coefficient with air density and flow velocity is considerably more pronounced than expected. These anomalies are quite probably unique to the orbiter's air vent system and structural configuration; therefore, it appears that IML convection cooling is more complex than theory indicates but extrapolation of OFT data to other STS entry environments can be justified. However, applying IML cooling for design of new spacecraft warrants caution.

Thermal analysis prediction capabilities are quite good when the environments are known. Analysis of flight data demonstrates this claim. Absence of flight data is evidenced in attempts to understand discrepancies between flight and analysis results. One example of this is not having adequate instrumentation to measure pressure gradients in high Δp regions of the orbiter. Assessment of high Δp gap heating requires this information. More pressure instrumentation should have been located in high Δp regions of the orbiter. Also, more surface and structure thermocouples should have been placed in areas where local heating environments are difficult to predict (e.g., elevon spill regions and penetrations).

REFERENCES

1. Dotts, R. L.; Battley, H. H.; Hughes, J. T.; and Neuenschwander, W. E.: Space Shuttle Orbiter Reusable Surface Insulation Subsystem Thermal Performance. AIAA Paper 82-0005, Jan. 1982.

2. Curry, D. M.; Cunningham, J. A.; and Frahm, J. R.: Space Shuttle Orbiter Leading Edge Structural Subsystem Thermal Performance. AIAA Paper 82-0004, Jan. 1982.

3. Dotts, R. L.; Smith, J. A.; and Tillian, D. J.: Space Shuttle Orbiter Reusable Surface Insulation Flight Results. Shuttle Performance: Lessons Learned, NASA CP-2283, Part 2, 1983, pp. 949-966.

4. Curry, D. M.; Johnson, D. W.; and Kelly, R. E.: Space Shuttle Orbiter Leading Edge Flight Performance Compared to Design Goals. Shuttle Performance: Lessons Learned, NASA CP-2283, Part 2, 1983, pp. 1065-1082.

5. Cunningham, J. A.; and Haney, J. W., Jr.: Space Shuttle Wing Leading Edge Heating Environment Prediction Derived From Development Flight Data. Shuttle Performance: Lessons Learned, NASA CP-2283, Part 2, 1983, pp. 1083-1110.

TABLE I.- SUMMARY OF TPS PENETRATIONS

Type	Quantity	Type	Quantity
Actuated doors and hatches		External window assemblies	9
• Landing gear	3		
• Payload bay (segments)	8	Structural element interface areas	4
• Crew hatches	3		
• Structural vents	18	Antennas	22
• Flipper doors	30		
• External tank	2	Exposed umbilical connectors	87
• Star tracker	2		
• Air data probe	2	Fixed panels and doors	295
Aero surfaces assemblies			
• Elevons	4	Miscellaneous singularities	
• Body flap	1	• External hinges and latches	36
• Rudder/speed brake (segments)	4	• Hot structure panels	37
		• Attach, hoist, and jack points	315
Engines			
• Main	3	• Vertical tail leading edge	1
• OMS	2		
• RCS	44	• Emergency access releases	3
		• Passive air vents	6
Vents and drains	54	• External light	1

TABLE II.- TYPICAL TPS TEMPERATURE CRITERIA

Material	TPS Elements	Temperature Limit (°F)*
Aluminum (2XXX, 6XXX)	Structure brackets, etc.	350
Beryllium	Heat sinks	1000
Borosilicate glass	HRSI coating	2300
	LRSI coating (low α_s/ε)	1200
Ceramic fabric (AB-312)	Thermal barrier, gap filler, and insulation covers	2000
Ceramic fibers, bulk		
(Dynaflex)	Batt insulation	2600
(Saffil)	Thermal barrier and gap filler	2000
Columbium, coated	Hub seals, nozzles, and flanges	2500
Fluoroelastomer (Viton)	Seals	500
Nickel alloy (Inconel 6XX)	Hot structure, seals, etc.	1400
Nylon (Nomex) felt	Filler bar	800
	FRSI	700
	SIP (for standard size tiles)	550
Polyimide/glass laminate	Isolators, brackets, etc.	600
Silica fibers, rigidized	Standard (ρ = 9 pcf) tiles	2300
	High-density (ρ = 22 pcf) tiles	2300
Steel (21-6-9)	Vents, brackets, etc.	900
(3XX)		1200
Titanium (6AL-4V)	Hot structure, brackets, etc.	800

*For 100 missions; higher values acceptable for limited missions or by specific tests, lower values specified in some system applications.

TABLE III.- TPS POSTFLIGHT ANOMALY OBSERVATIONS

Item	Location Code**
Tile slumping (overtemperature)*	A
Thermal barrier degradation*	B
Scorched FRSI*	C
Structural overtemperature	D
Tile erosion*	E
Gap filler degradation*	F
Gap filler leakage	G
Burned elevon cove insulation	H
Scorched filler bars	Random on lower surfaces

*Easily detectable by visual inspection of the OML
**Refer to Figure 15

TABLE IV.- SCORCHED FILLER BAR

Flight	Total	CAT. 1	CAT. 2	CAT. 3	Tiles Removed*	Comments
STS-1	614	113	269	232	246	Early trans (gouge) First flight
STS-2	360	130	194	36	47	
STS-3	219	73	117	29	34	
STS-4	478	238	224	16	16	Early trans (PUPO)

*Because of scorched filler bars

CAT. 1: 950 → 1100°F

CAT. 2: 1100 → 1375°F

CAT. 3: > 1375°F

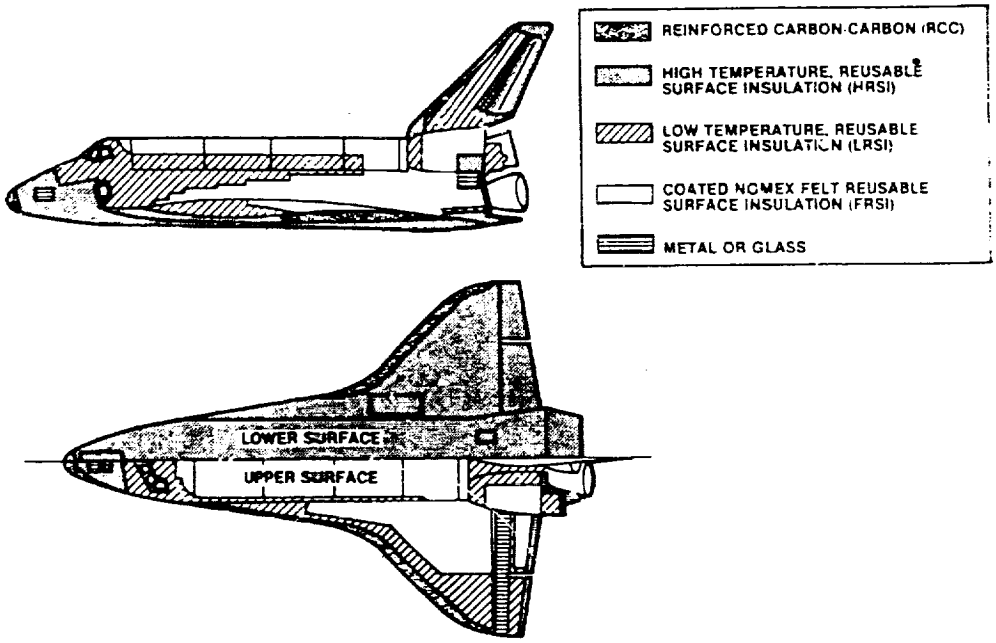

Figure 1.- Thermal protection system (Orbiter 102).

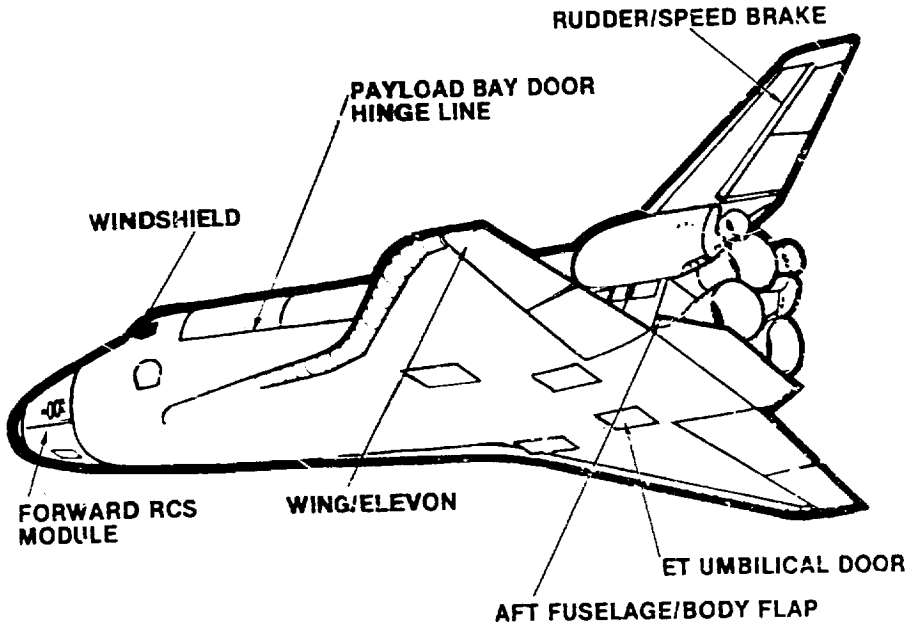

Figure 2.- Typical TPS penetrations.

TILE SYSTEM

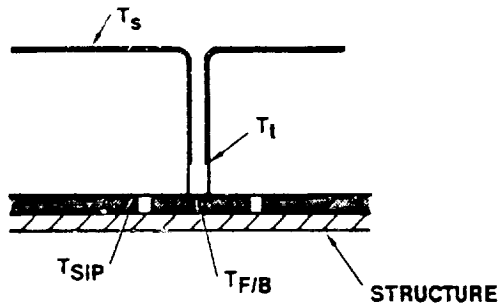

TILES:
- T_s = 2300°F HRSI, 1200°F LRSI
- T_t = 1050°F
- $T_{F/B}$ = 800°F
- T_{SIP} = 550°F TYPICAL, 600°F MINI TILES

FRSI:
- T_s = 750°F ASCENT, 700°F ENTRY
- T_{RTV} = 550°F

PRIMARY STRUCTURE: 350°F

FRSI

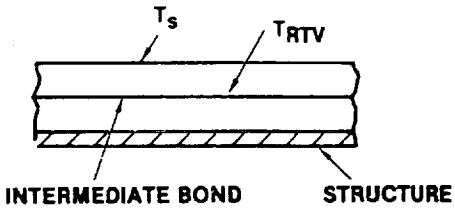

Figure 3.- 100-mission temperature allowables (acreage).

ACREAGE			
INSTALLATION TYPE	NUMBER OF INSTALLATIONS	TEMPERATURE MEASUREMENTS PER INSTALLATION	TOTAL TEMPERATURE MEASUREMENTS
SURFACE TEMPERATURES	177	1	177
SURFACE/SKIN TEMPERATURES	11	2	22
SKIN STRUCTURE TEMPERATURE	61	1	61
INTERNAL STRUCTURE TEMPERATURE	67	1	67
CENTER-TILE PLUG			
LOWER SURFACE	13	5	65
UPPER SURFACE	2	5	10
	3	4	12
BASE HEAT SHIELD	1	5	5
TILE SIDEWALL TEMPERATURE			
TILE JOINT ARRAY	1	13	13
	5	3	45
TRAILING EDGES	11	5	55
BASE HEAT SHIELD	1	5	5
		TOTAL	537

PENETRATIONS	
INSTALLATION TYPE	NUMBER OF TEMPERATURE MEASUREMENTS
EXTERNAL TANK ATTACHMENT	2
REACTION CONTROL SYSTEM	5
WINDOWS	3
VENT AND DUMP	7
ACCESS PANELS	3
PAYLOAD BAY DOORS	16
OTHER DOORS (MAIN LANDING GEAR, ET, STAR TRACKER)	13
WING ELEVON DYNAMIC SEALS	18
BODY FLAP DYNAMIC SEALS	7
VERTICAL TAIL DYNAMIC SEALS	12
TOTAL	88

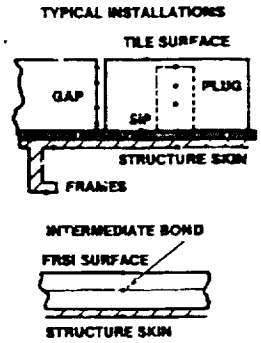

Figure 4.- Development flight instrumentation.

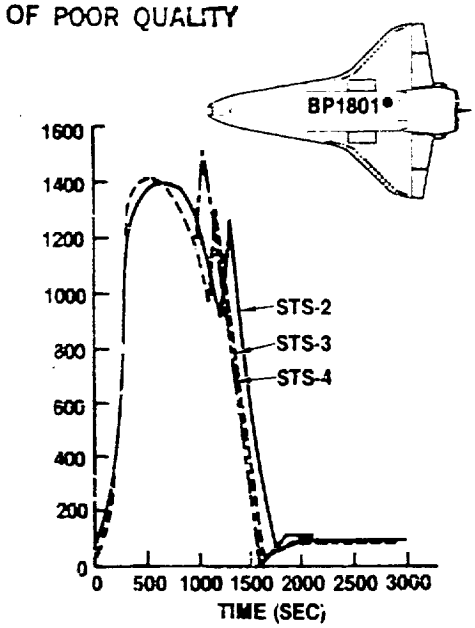

Figure 5.- Representative lower surface temperature response.

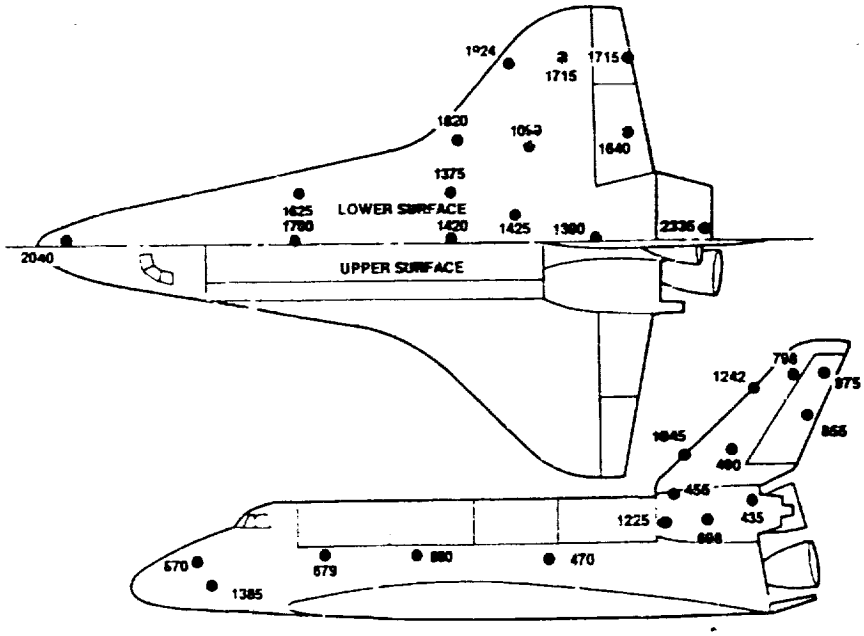

Figure 6.- STS-2 peak surface temperatures (^{o}F).

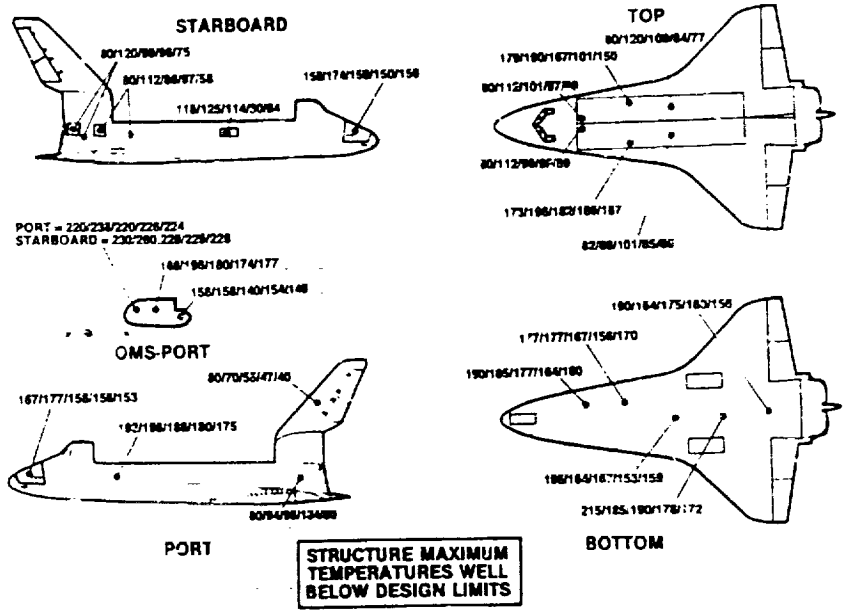

Figure 7.- STS-2 flight temperatures (^{o}F).

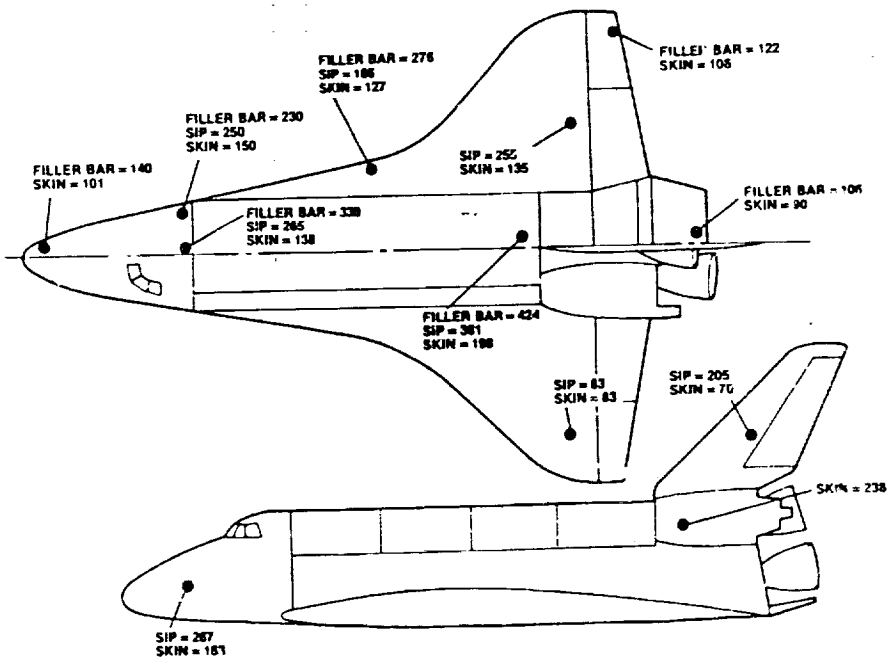

Figure 8.- Structure maximum temperatures (^{o}F).

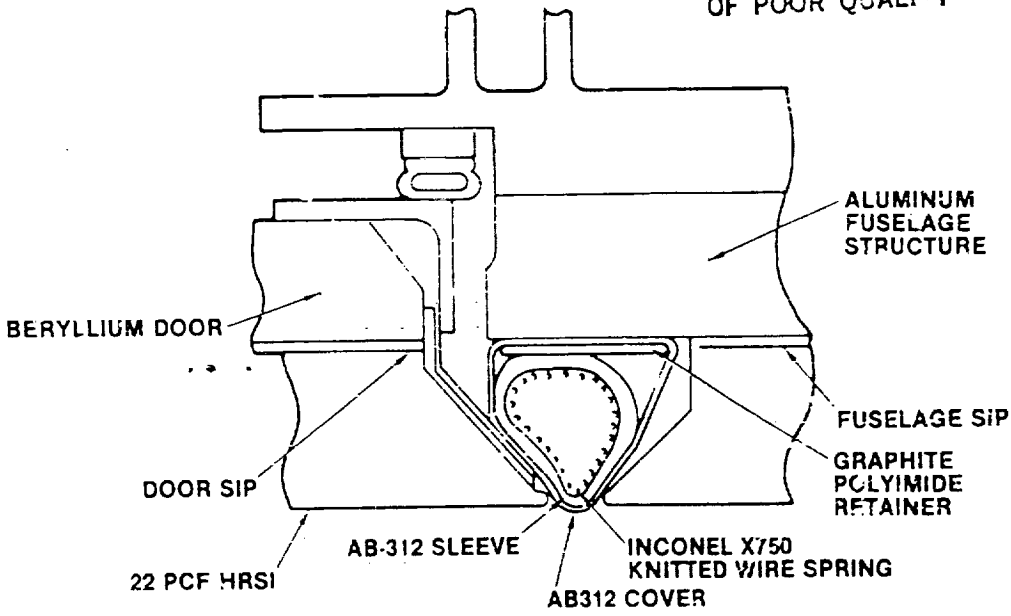

Figure 9.- ET/orbiter umbilical door.

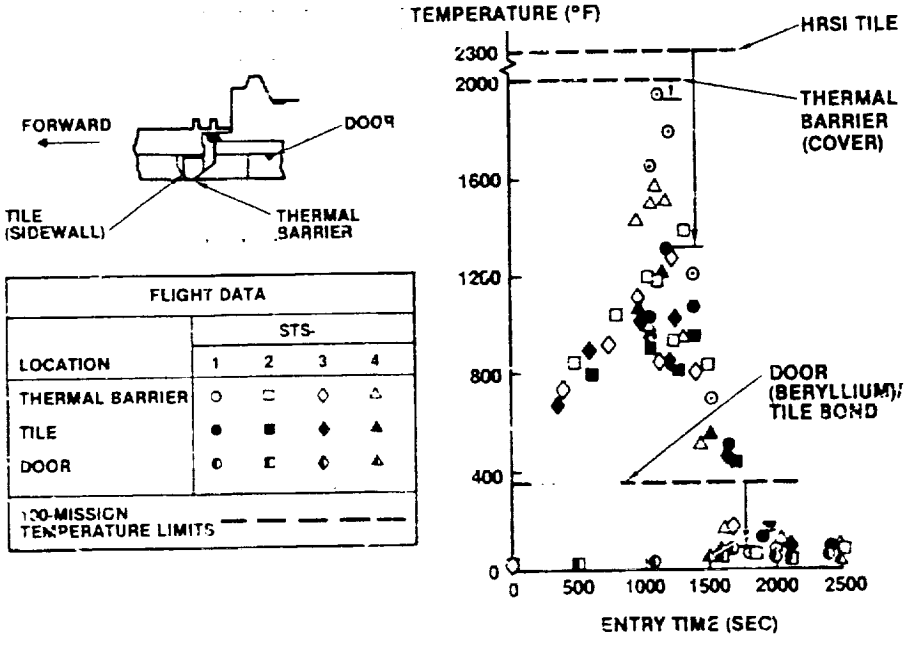

Figure 10.- ET door temperatures.

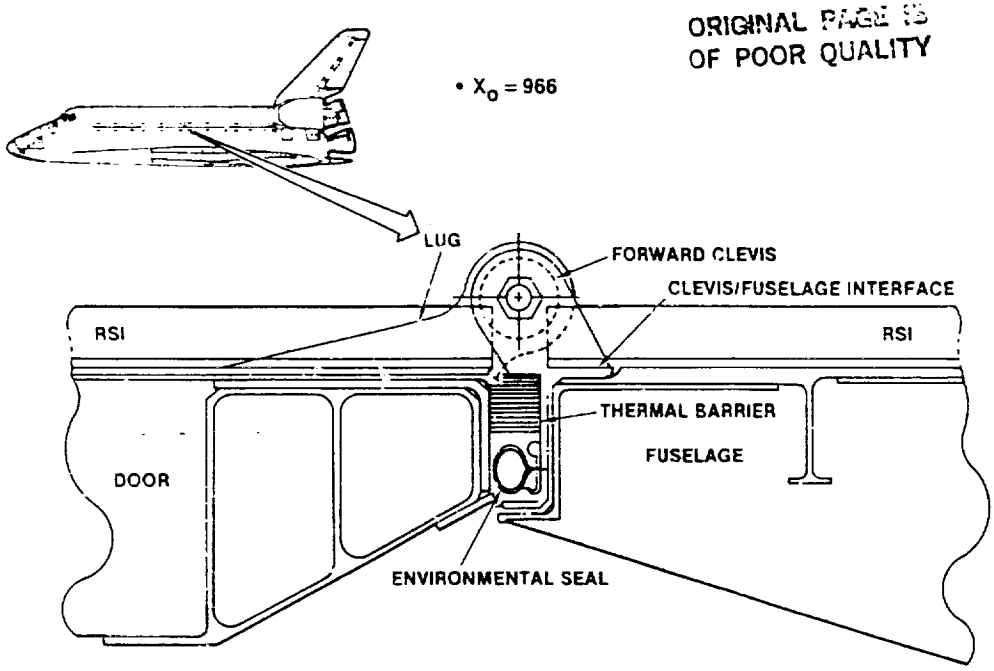

Figure 11.- Unprotected PLB door hinge.

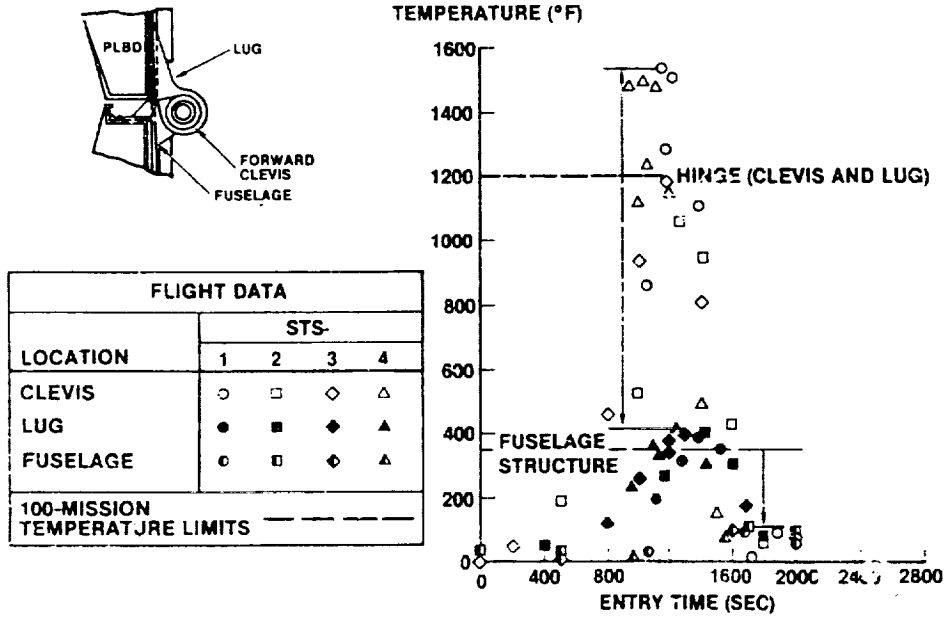

Figure 12.- PLB door bare hinge temperatures.

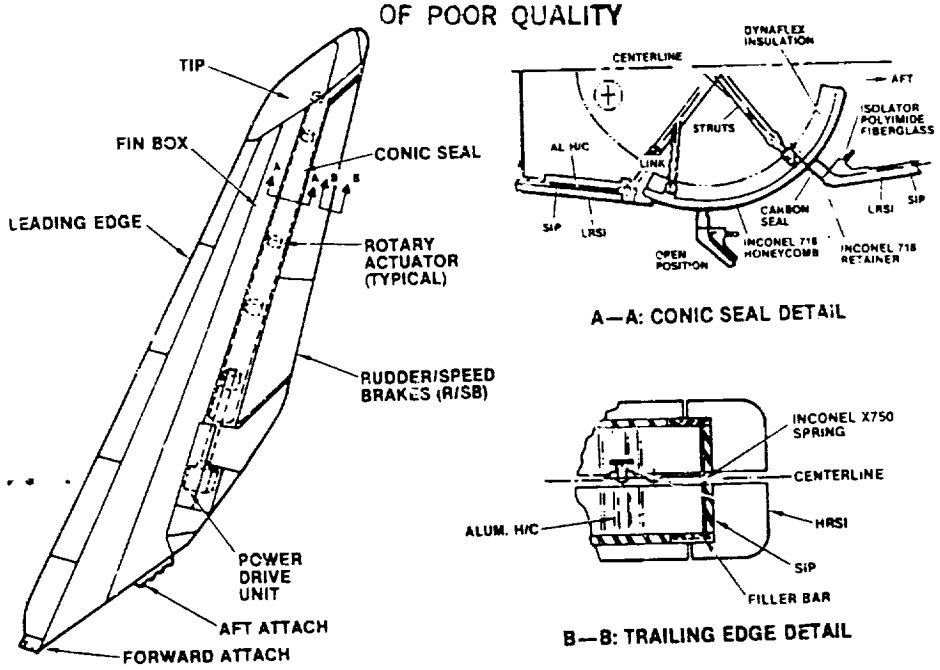

Figure 13.- Vertical tail.

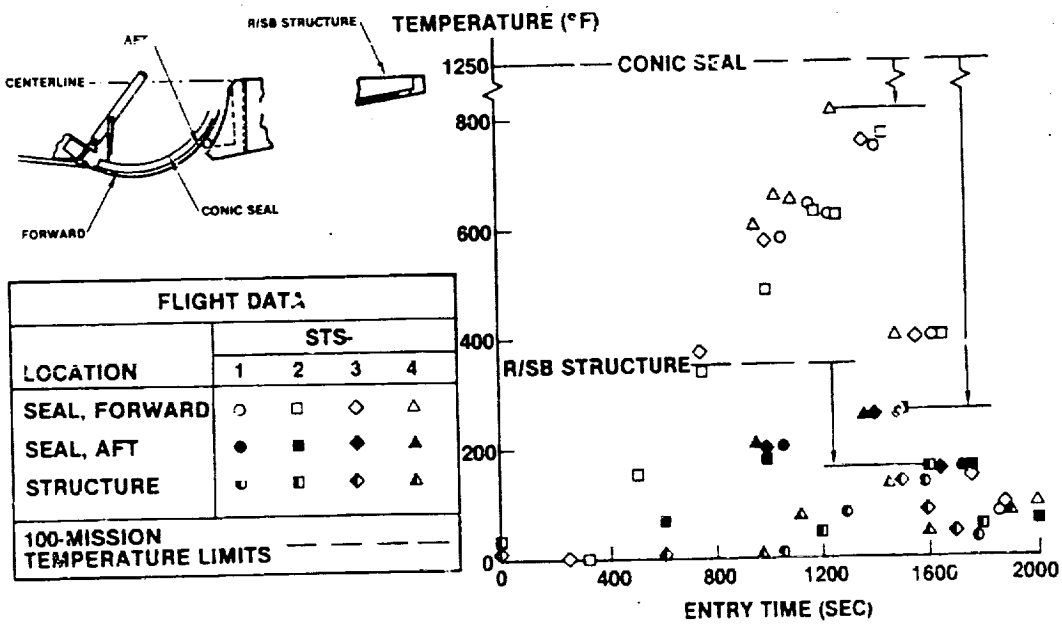

Figure 14.- Conic seal and rudder/speed brake structure temperatures.

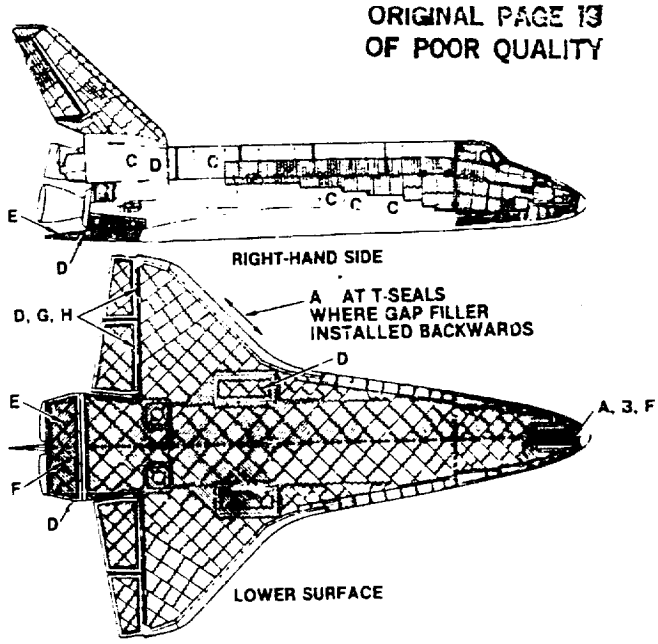

Figure 15.- Locations of significant TPS degradation.

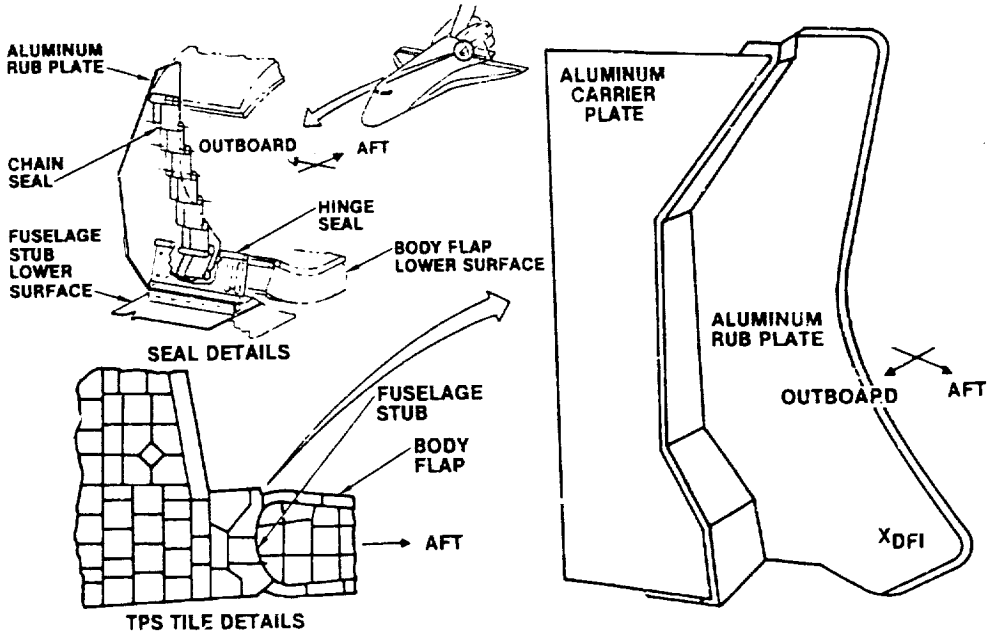

Figure 16.- Stub and body flap.

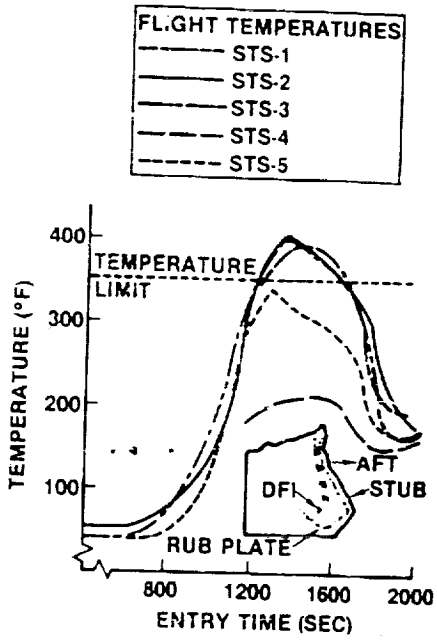

POSTFLIGHT CORRECTIVE ACTIONS

- STS-1
  - ADDED AMES GAP FILLER BETWEEN STUB TILES ON LOWER SURFACE
- STS-2
  - REMOVED CARRIER PANEL TILES (SIDE OF STUB)
  - REPLACED CHARRED/MISSING FILLER BAR
  - PAD GAP FILLER REBONDED
- STS-3
  - REMOVED CARRIER PANEL TILES
  - REMADE TWO LOWER SURFACE TILES TO REMOVE FORWARD-FACING STEP
  - ADDED AB312 ROPE FLOW BARRIER, NEW GAP FILLER AND RTV
- STS-4
  - NONE
- STS-5
  - CARRIER PANELS OFF AWAITING TILE AND GAP FILLER MODIFICATIONS

Figure 17.- Body flap rub plate anomaly.

Figure 18.- STS-2 postflight condition of fuselage stub.

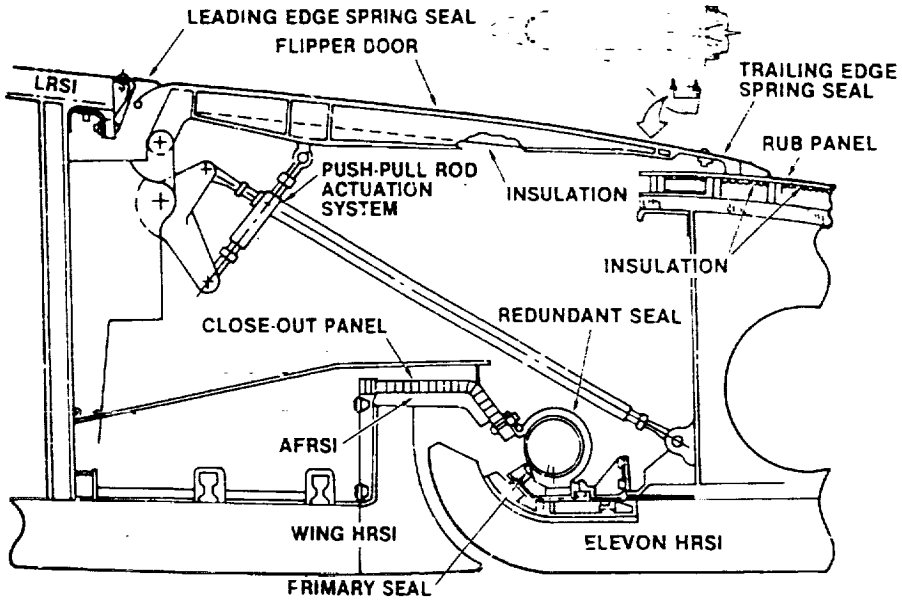

Figure 19.- Elevon seal system: design configuration.

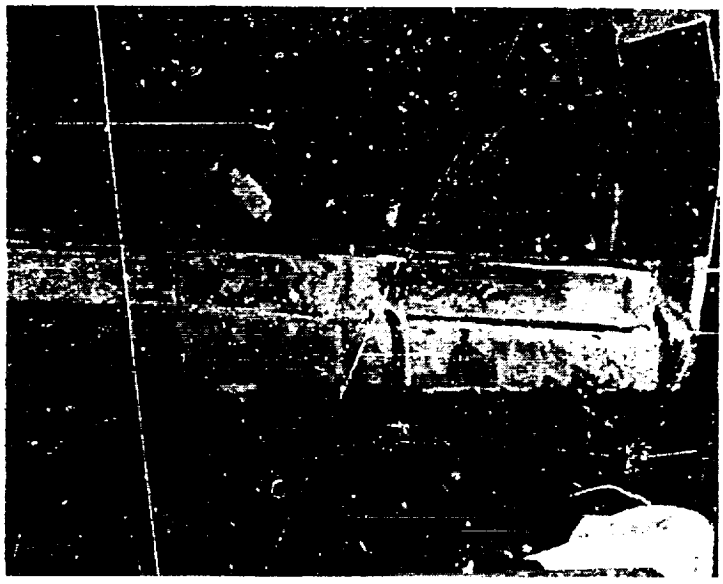

Figure 20.- Elevon lower cove close-out panels after STS-1.

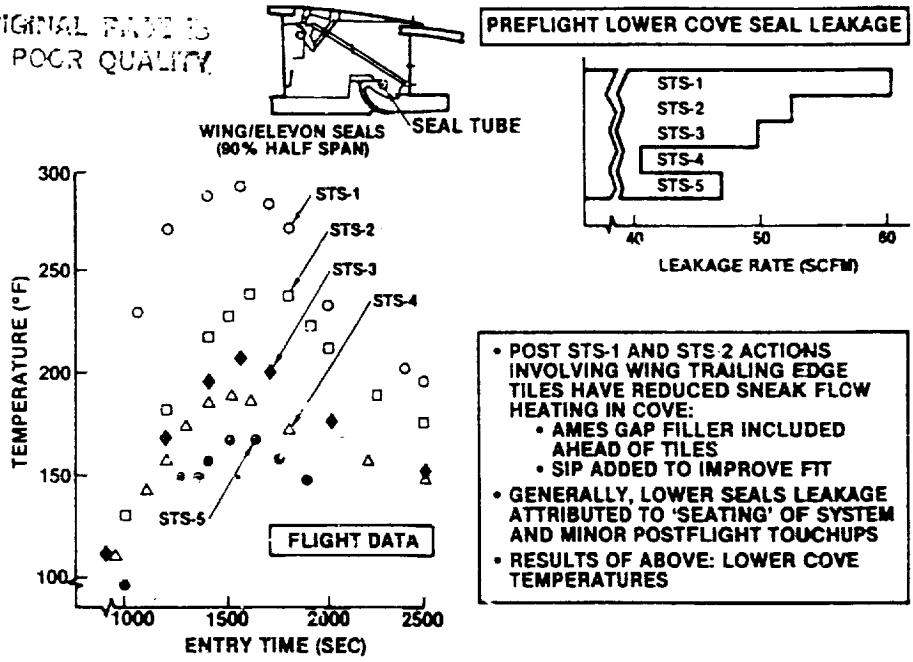

Figure 21.- Trends in the elevon lower case.

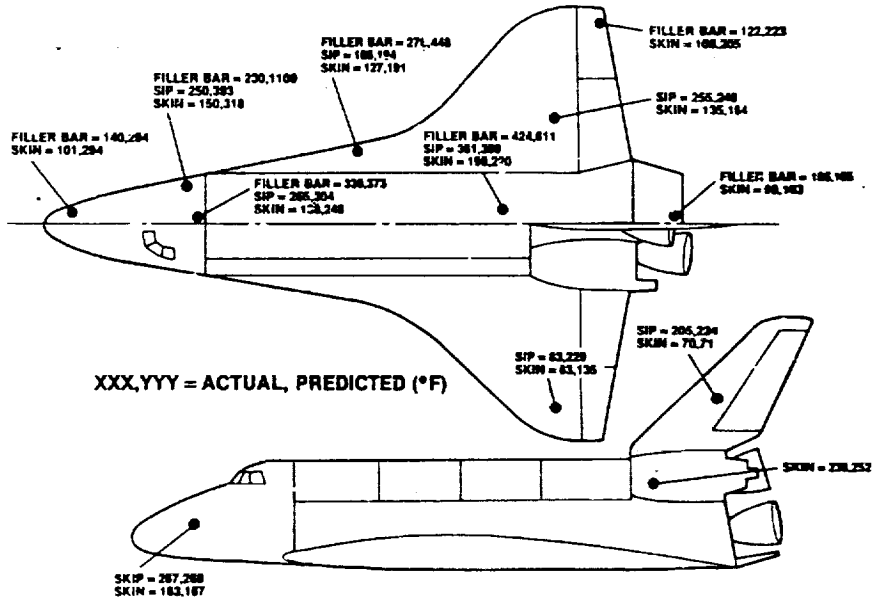

Figure 22.- Comparison of STS-2 flight and postflight analysis temperatures.

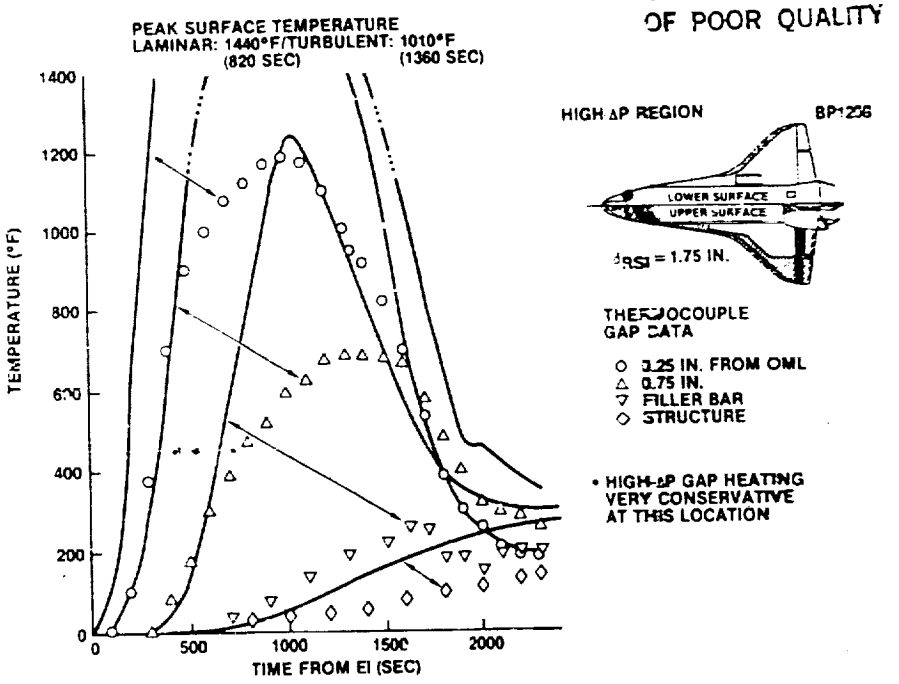

Figure 23.- Comparison of design method with STS-2 flight temperatures (high Δp location).

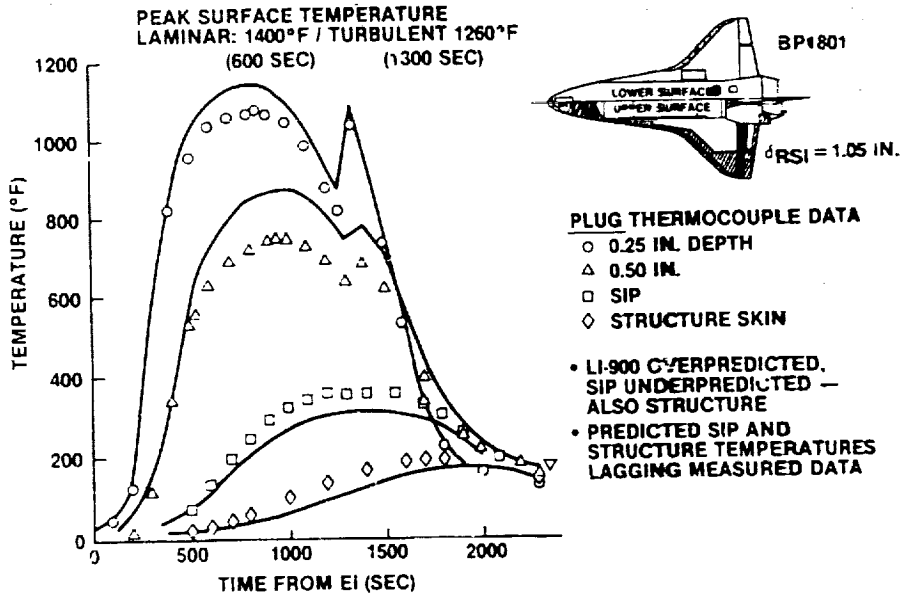

Figure 24.- Comparison of design method with STS-2 flight temperatures (plug thermocouples).

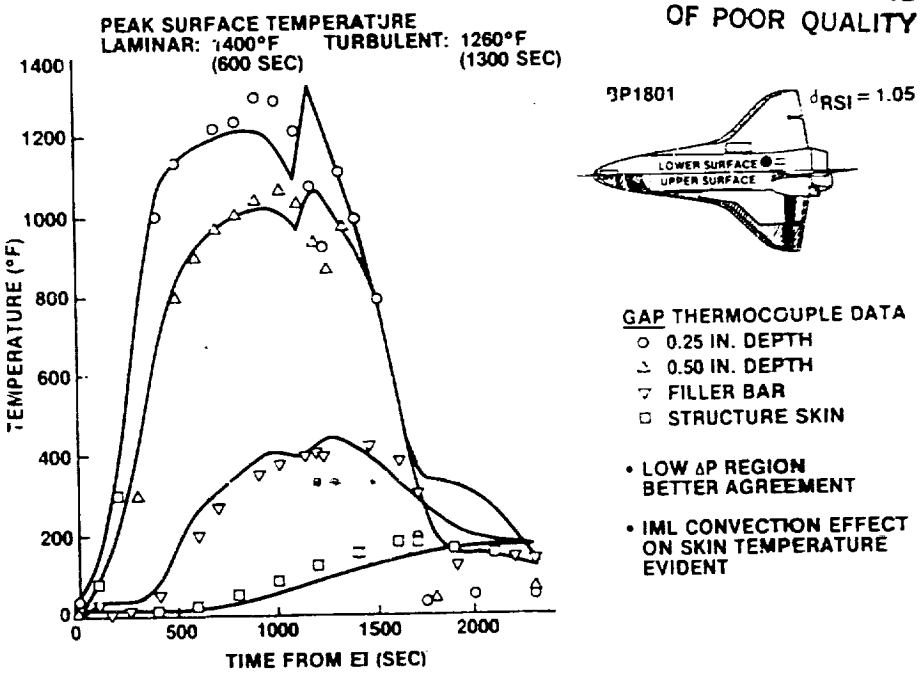

Figure 25.- Comparison of design method with STS-2 flight temperatures (gap thermocouples).

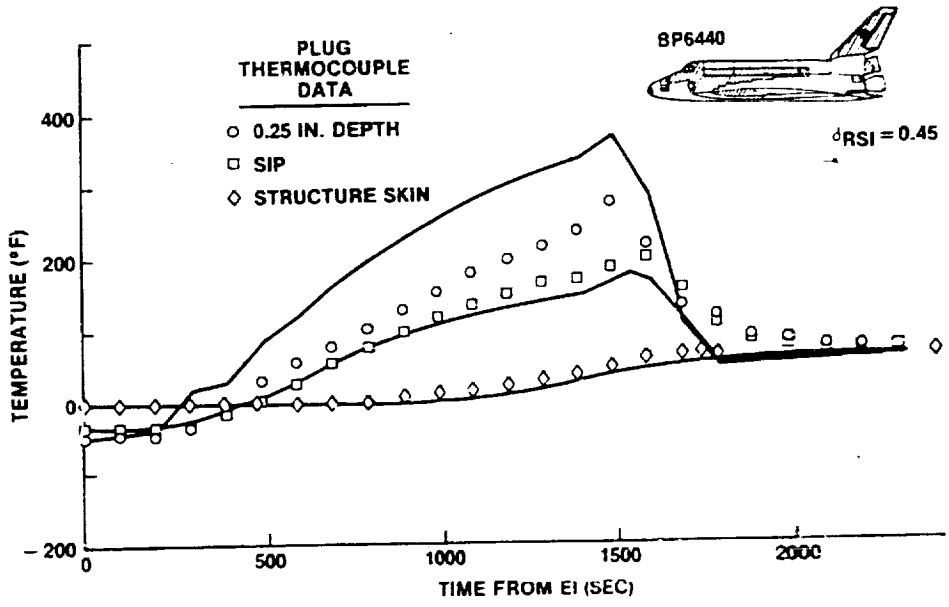

Figure 26.- Comparison of design method with STS-2 flight temperature (LRSI location).

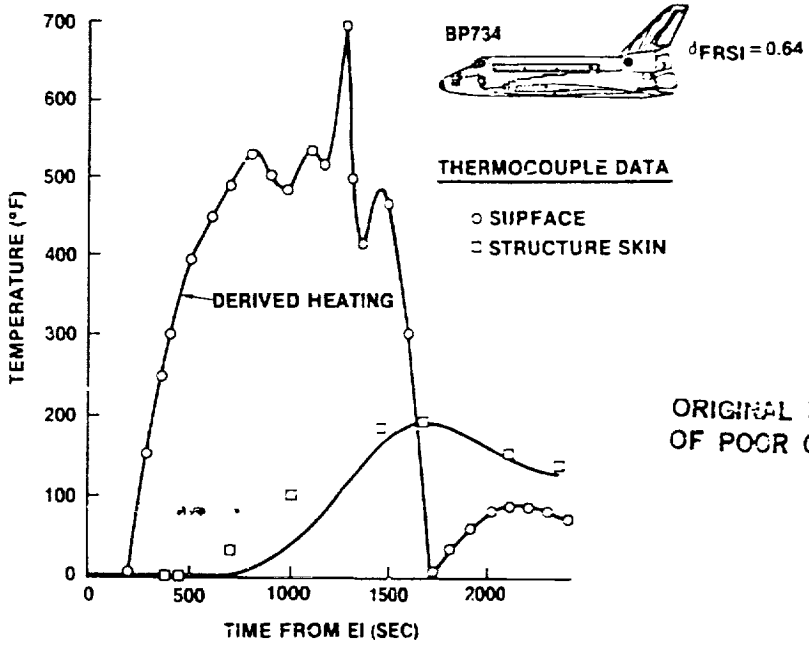

Figure 27.- Comparison of design method with STS-2 flight temperature (FRSI location).

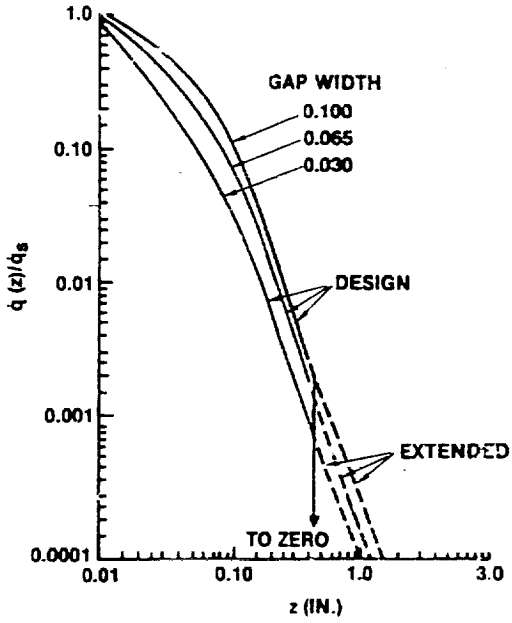

Figure 28.- Low pressure gradient gap heating distribution.

n = 1.6 FROM CORRELATION OF STS-2 DATA

h′ = 0.10 FOR UNINSULATED STRUCTURE
h′ = 0.07 FOR INSULATED STRUCTURE
} FROM EXAMINATION OF T STRUCTURE DATA

V/V′ FROM INTERPRETATION OF FLIGHT DATA

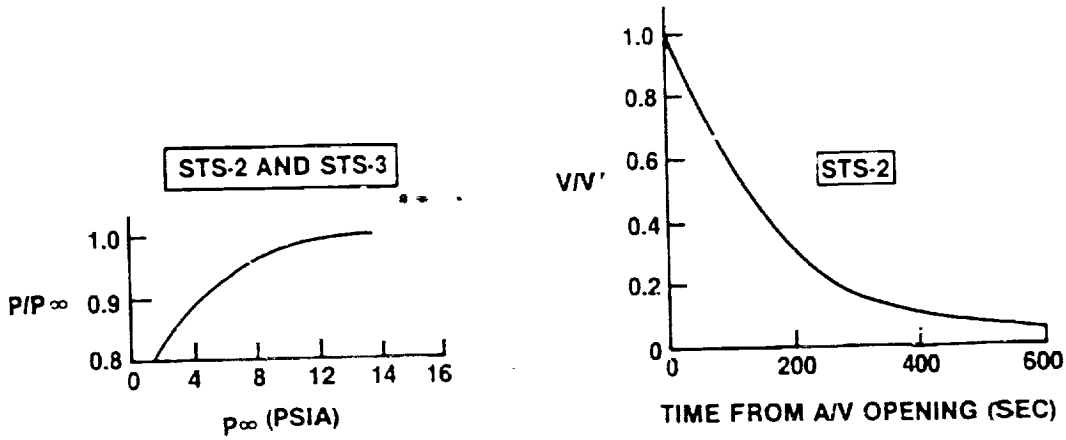

Figure 29.- Preliminary IML convection data.

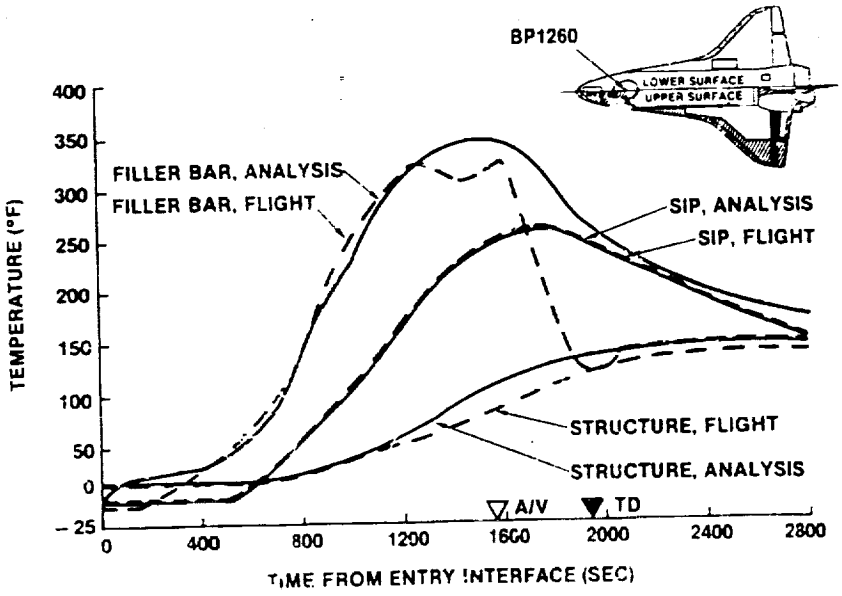

Figure 30.- Comparison of improved method with STS-2 flight temperatures (lower fuselage, IML insulated).

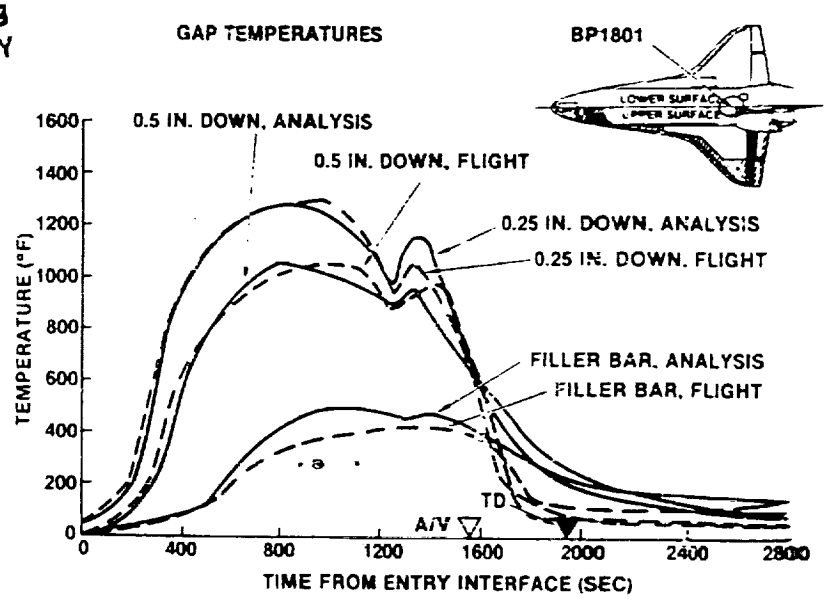

Figure 31.- Comparison of improved method with STS-2 flight temperatures (lower fuselage, IML not insulated).

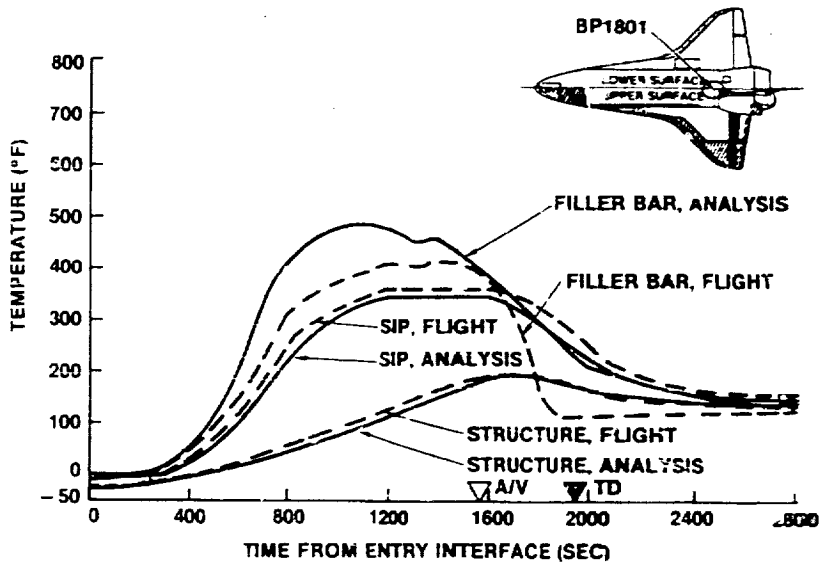

Figure 32.- Additional comparison of improved method with STS-2 flight temperatures (lower fuselage, IML not insulated).

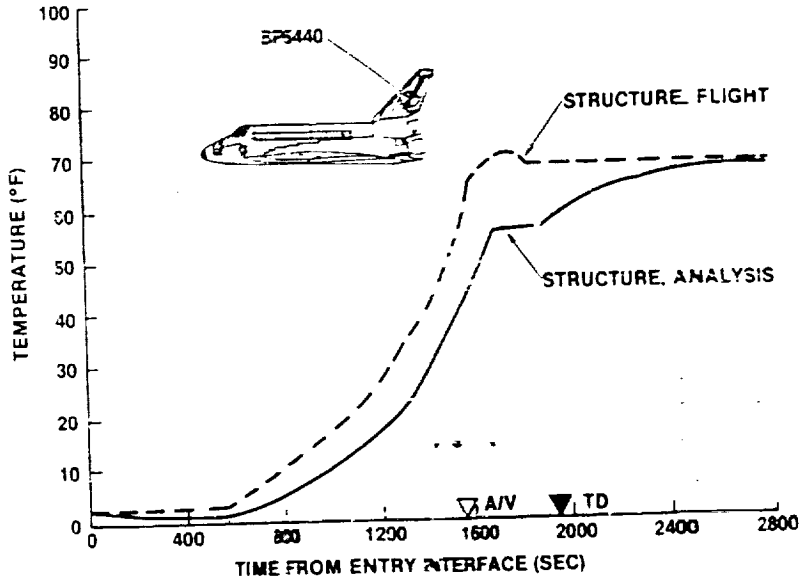

Figure 33.- Comparison of improved method with STS-2 flight temperatures (LFSI location).

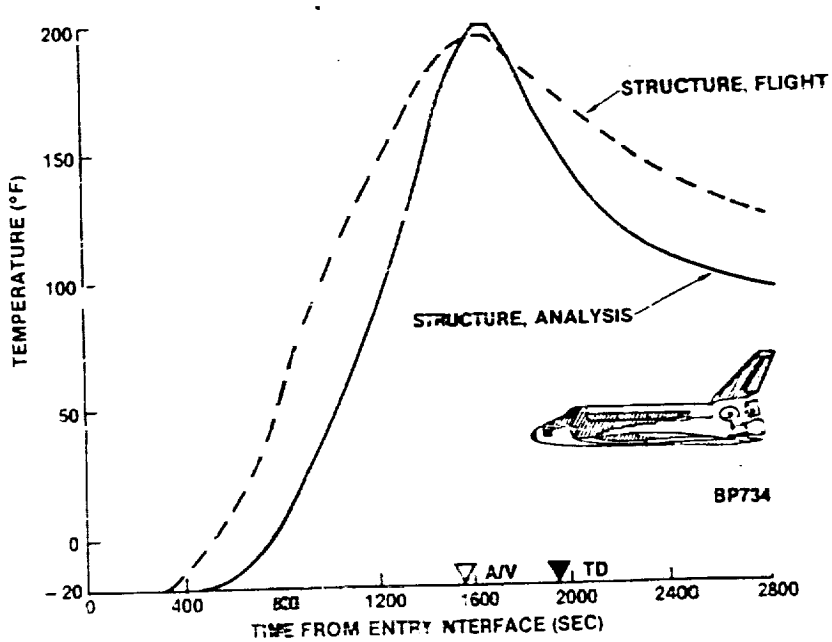

Figure 34.- Comparison of improved method with STS-2 flight temperatures (RFSI location).

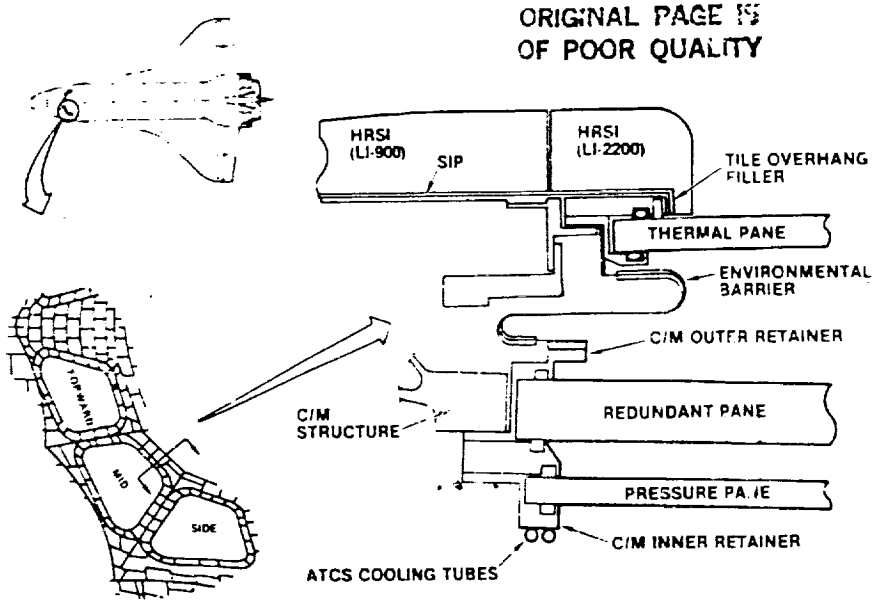

Figure 35.- Windshield design configuration.

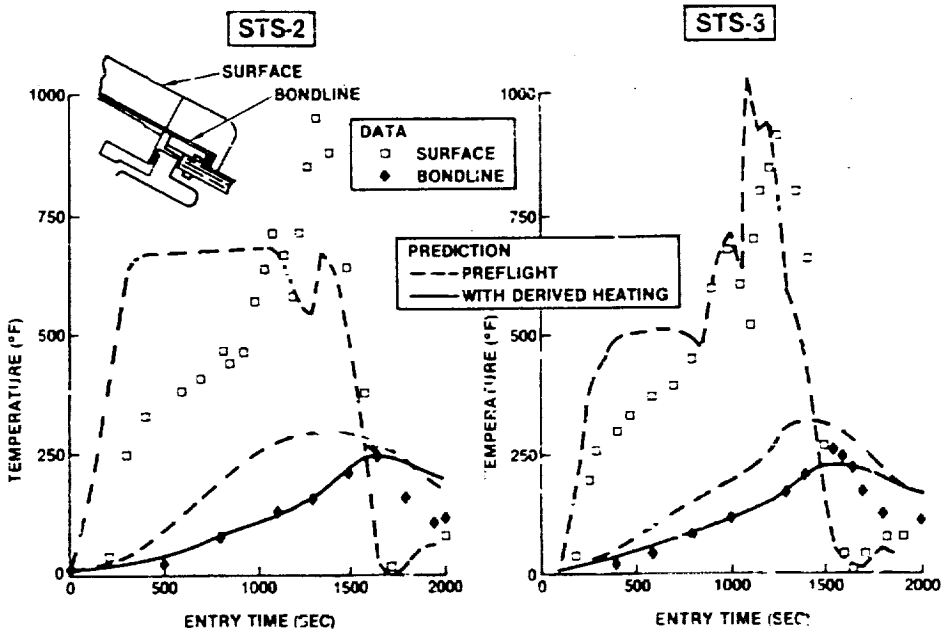

Figure 36.- Windshield modeling improvements.

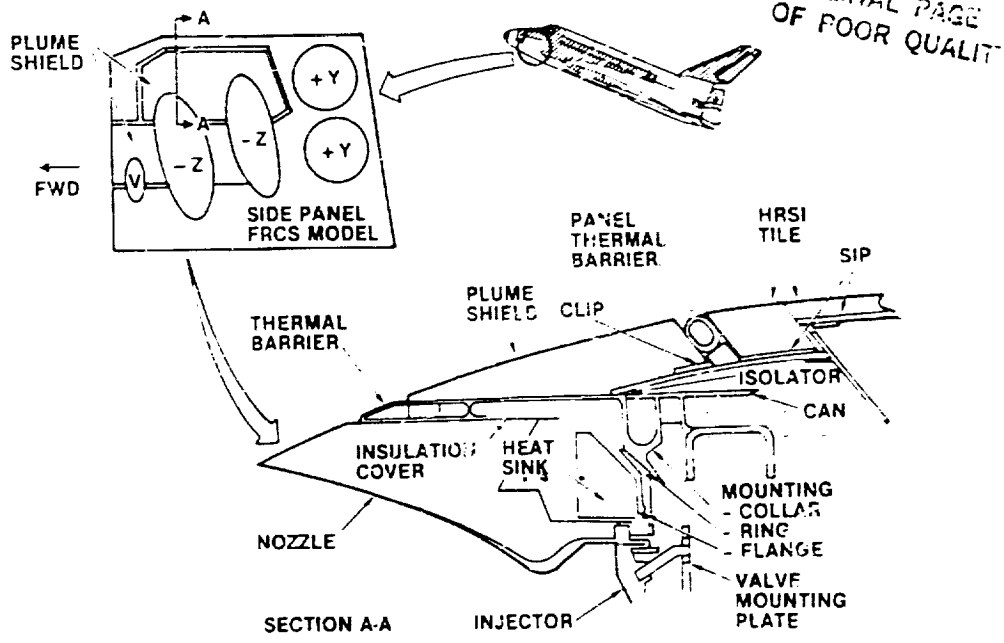

Figure 37.- FRCS-Z thruster design installation.

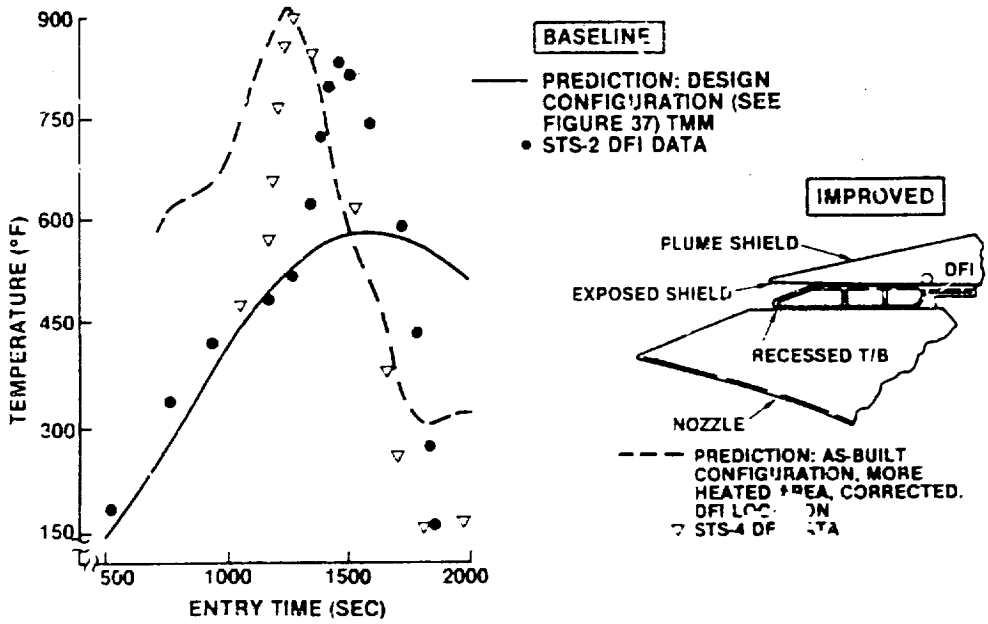

Figure 38.- FRCS thruster modeling improvements.

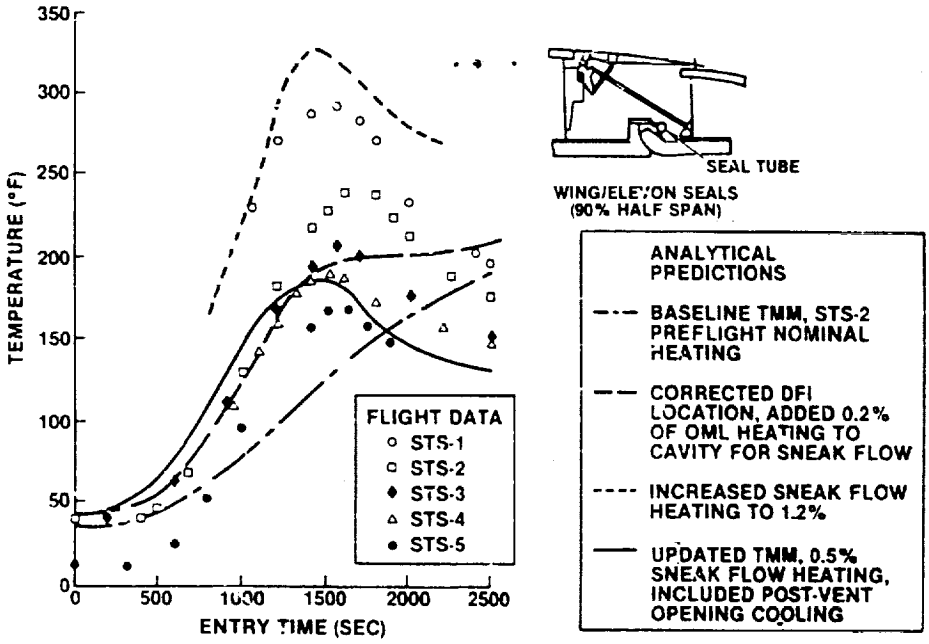

Figure 39.- Elevon lower cove modeling improvements.